ANALYSIS OF KINETICS PARAMETERS ON T CELL RECOGNITION TO VIRAL INFECTION

A Dissertation
Presented to
The Academic Faculty

by

Prithiviraj Jothikumar

In Partial Fulfillment
of the Requirements for the Degree
Doctor of Philosophy in the
School of Biomedical Engineering

Georgia Institute of Technology
August 2016

ANALYSIS OF KINETICS PARAMETERS ON T CELL RECOGNITION TO VIRAL INFECTION

Approved by:

Dr. Cheng Zhu, Advisor
Department of Biomedical Engineering
Georgia Institute of Technology and Emory University

Dr. Arash Grakoui
Department of Medicine, Division of Infectious Diseases
Emory University School of Medicine

Dr. Krishnendu Roy
Department of Biomedical Engineering
Georgia Institute of Technology and Emory University

Dr. Hang Lu
Department of Chemical Engineering
Georgia Institute of Technology

Dr. Manu Platt
Department of Biomedical Engineering
Georgia Institute of Technology and Emory University

Date Approved: July 14, 2016

To my unconditionally loving family

ACKNOWLEDGEMENTS

This work in its entirety involved multiple people. First and foremost, I wish to thank my advisor and mentor, Dr. Cheng Zhu, for giving me the opportunity to work on this project that is close to my heart and my utmost interests. With his guidance and support, is truly why I was motivated and challenged to explore in my studies and his encouragement to always to try new things in science has really pushed these projects to new heights. I would like to also thank Dr. Arash Grakoui, who has been an unofficial co-advisor on my projects associated with my thesis. His support and opportunity has provided me with great in-depth exposure to the field of immunology. I also want to sincerely thank my committee members Dr. Hang Lu, Dr. Manu Platt and Dr. Krishnendu Roy for their wonderful discussion and support on these projects to help me improve on all standards.

I wish to sincerely thank, Dr. Young-Jin Seo, who has worked enormously with me on the LCMV study and the entirety of the project cannot be accomplished without his invaluable contributions. Discussion and working with Dr. Seo has really opened up multiple avenues on the LCMV work. I wish to thank Paul Cardenas-Lizana, a colleague and a collaborator on the CMV study for his inputs and suggestions. Paul's discussion on how to correlate experiments and simulation has provided unique discussion. I want to thank Dr. Jinsung Hong, Dr. Brett Mendel, Dr. Sergey Pryshchep, and William Rittase for the invaluable discussion that helped progress my research and understanding over the time. I also would like to thank the following for the great support, mentoring me in various techniques and providing reagents: Dr. Loice Chingozha, Dr. Yunfeng Chen,

Elizabeth Elrod, Chenghao Ge, and Dr. Chris Ibegbu, Kaitao Li, Dr. Baoyu Liu, and Fangyuan Zhou. Additionally, I wanted to thank the following for the numerous discussion that helped me understand various topics and exposure to different fields: Dr. Arlene Stecenko and Dr. Nael McCarty on Cystic Fibrosis project; Dr. Jon Yewdell and Dr. Suman Das on influenza project; Dr. Ning Jiang, Dr. Wei Chen, Dr. Shashidhara Murthy, and Dr. Periasamy Selvaraj on Fc-γ receptors; Dr. Susan Thomas on tumor project; Dr. Ke Bai on HIV VLP project. I like to thank the following colleagues for their great and invaluable discussion over the years: Dr. Victoria Best, Vaclav Beranek, Dr. Jack Wei Chen, Dr. Arnold Ju, Jiexi Liao, Dr. Hyun-Jung Lee, Dr. Zhenahi Li, Aryn Price, Aaron Rosado, Muaz Rushdi, Dr. Sanjeevi Sivasankar, Dana Tedesco, Dr. Manoj Thapa, Dr. Vijayakumar Velu, Chad Williams, Ning Wu, and Zhou Yuan, Dr. Veronika Zarnitsyna. I wanted to give special thanks to Ms. Larissa Doudy who has committed a friendly environment in the lab and has helped me countless times with any help I need from learning the ropes of the lab environment to listening patiently with all my progress during my graduate studies.

I would also like to thank Dr. Esfandiar Behravesh, Paul Fincannon, Sally Gerrish, Sara Kunicki, Dr. Josepsh LeDoux, and Laura Paige for their continuous support for both towards and outside my research. I also like to thank my friends from undergrad who came along with me to grad school at Georgia Tech and their continued support through my graduate studies: Nishant Zachariah, Christa Caesar and Mike Weiler. I also wanted to thank the technical core facility staff of IBB and EBB at Georgia Tech for allowing me to book the sorter multiple times and teaching: Nadia Boguslavsky, Andrew Shaw, and Steve Woodard.

TABLE OF CONTENTS

LIST OF FIGURES

Page

LIST OF SYMBOLS AND ABBREVIATIONS

2D	Two dimension(al)
3D	Three dimension(al)
A_cK_a	Effective binding affinity
APC	Antigen presenting cell or Allophycocyanin
BFP	Biomembrance force probe
BSA	Bovine serum albumin
CMV	Cytomegalovirus
CTL	Cytotoxic lymphocyte
EAS-45	Experimental additive solutions 45
EBV	Epstein Barr virus
FACS	Fluorescence activated cell sorting
FRET	Fluorescence resonance energy transfer
FBS	Fetal bovine serum
gp33	Glycoprotein 33
HCV	Hepatitis c virus
HIV	Human immunodeficiency virus
ITAM	Immunoreceptor tyrosine-based motifs
k	Stiffness or spring constant
K_a	Affinity
k_{off}	Off-rate
LAT	Linker for activation of T cells
LCK	Lymphocyte-specific protein tyrosine kinase
LCMV	Lymphocytic choriomeningitis virus

MHC	Major histocompatibility complex
MPEC	Memory precursor effector cell
m_l	Ligand site density
m_r	Receptor site density
p	peptide
P_a	Adhesion frequency
PBS	Phosphate buffered saline
PD-1	Programmed death 1
PE	Phycoerythrin
pMHC	Peptide major histocompatibility complex
RBC	Red blood cell
RP	Red pulp
RT	Room temperature
s	Second
SEM	Standard error of the mean
SLEC	Short lived effector cell
SLO	Secondary lymphoid organ
SLP-76	Src-homology-2-domain-containing leukocyte protein of 76kDa
TCR	T cell receptor
WP	White pulp
ZAP-70	Zeta-chain-associated protein kinase 70

SUMMARY

T cell plays an important role in clearance of viral infections and development of memory population for a rapid immune response in the case of secondary infections. T cells utilize T cell receptor (TCR) to recognize viral antigens in the form of peptide major histocompatibility complex (pMHC) as its ligand. When viral mutations occur, TCR recognition is impaired for its ligand and in result, lowers immune cell lytic response. Conventionally, TCR binding kinetics to its ligands is linked to TCR binding propensity stemming from 3D assays, providing numerical values in relation to its strength. However, characterizing the interaction of viral variant peptides to TCR is poorly understood and providing a unique perspective in understanding the interaction provides potential solutions to vaccine development, especially for chronic viral infections. In this study, we characterize Cytomegalovirus (CMV)-specific T cell 2D effective binding affinity to both WT and viral variants. Additionally, we characterized to elucidate the importance of specific amino acids found on the peptide influences recognition, thereby potentially bridging gap to understand the mechanics of how specific recognition motifs influence functionality. As T cell gets activated following peptide recognition, multiple signaling pathways take place in order to invoke an effective functional output. To invoke such a response, T cells first translate from naïve to activated state and then returning to homeostasis over the course of an immune response. Although the entire process takes several days, how recognition dynamics is influenced in the context of viral clearance and how that leads into developing memory population has not been fully elucidated. To understand these phenomenon, we primarily evaluated a single transgenic T cell

population over the course of an acute lymphocytic choriomeningitis virus (LCMV) viral infection to characterize and understand the dynamics of the T cell function and development that is influenced by organ compartmentalization. Our results highlight an important aspect on how TCR propensity is influenced by the microenvironments during viral clearance and in the occurrence of viral mutation, how characterizing TCR recognition provides new insights on impaired binding kinetic and functional profile.

CHAPTER 1

INTRODUCTION

Cytotoxic T Lymphocytes (CTL) recognition to viral peptides plays a crucial component in initiating multiple downstream signaling cascades to effectively eliminate viral pathogens found within the host, followed by which establishing a proper adaptive immune repertoire to fight off secondary infections. Different organs provide various functions to maintain homeostasis for the host and the secondary lymphoid organs (SLO) plays an important role in maintaining immune homeostasis stemming from T cell development and priming of CTL. Although the immunity of the host combats foreign pathogen to its utmost capability, on occasions, viral mutations takes place that leads to impaired T cell recognition, where no longer T cells cannot adapt to such mutations. In result, viral mutations stemming from selection pressure has the potential to non-effective CTL function, thereby contributing to the development of chronic infections. Current understanding of how viral mutations influence T cell function is characterized in detail with standard affinity measurement and has shown correlation to function, however, characterizing the interplay between interaction profile leading to impaired function has not been clearly elucidated. Furthermore, existing knowledge of microenvironments influencing CTL functions are not well characterized in the context of viral immunity and most importantly, how this response shapes up the viral adaptive immune system mediated via TCR dynamics and its environment has not been investigated. Therefore, the following objectives and specific aims are proposed to investigate the role of viral variant epitopes and microenvironmental influence on T cell kinetics utilizing 2D biophysical approach to analytically interpret new insights bridging engineering in the field of virology and immunology.

1.2 Objectives

The primary objective of this study is to understand and characterize the kinetics of TCR and its ligand, pMHC, of both the wild type and mutant variants of the viral epitope in the state of infection. In addition, during the course of infection, how antigen specific T cells from different compartments regulate $CD8^+$ T cells to its cognate viral epitope will also be characterized.

1.2 Aims and hypotheses

Aim 1. Characterize the relationship of wild type antigen-specific CD8+ T cell to a single antigen epitope and its mutant variants by biophysical assays and functional studies from cell line derived from virus-positive subject.

This aim will first validate the biophysical and functional characteristics of CMV epitope, specifically NLV epitope. This will be done using CD8+ T cell line derived from human subject pulsed with the wild type viral peptide. Biophysical parameters of this system will be derived by conducting micropipette adhesion frequency and Biomembrane Force Probe (BFP) to measure 2D affinity and characterize the effect different amino acid with different non-covalent bond observed, respectively. Functional study will be conducted by intracellular cytokine staining assay to validate and correlate the 2D biophysical results using plate-bound pMHC stimulation. This aim will primarily test the hypothesis whether the different mutations of the CMV epitopes will have different functional and binding characteristics. Just as various mutations of HCV epitopes have direct consequences to the outcome of the disease, we will mimic this scenario with CMV NLV epitope. However, this aim looks to understand how each wild type sequence and its mutant counterpart of CMV affects the binding kinetics. It is hypothesized that mutations at amino acid hot-spots of the antigenic peptide will exhibit low binding affinity and significantly impacted lifetime under various forces depicting viral variants

utilize to reduce or escape lytic function. Mutations pertaining to comparable or lower recognition will exhibit comparable or lower binding affinity and exhibit catch-bond like behavior compared to the wild type peptide. The interaction will be assessed between mutant variants pMHCs to CD8+ T cells derived from human subject pulsed with wild type viral peptide. The result of this will shed light into how T cell response is affected by different sequences of various epitopes of CMV and the insights obtained from this study could potentially be extrapolated to a more clinically relevant viral disease, such as HCV infection.

Aim 2. Assess the 2D kinetics of antigen specific T cells from circulation (RP) and tissue (WP) compartments from spleen of LCMV-infected mice over the course of the time and relate to functional role in the path to clear infection and adopting a memory repertoire.

This aim will test the hypothesis that infection will induce morphologically and functionally distinct spleen compartments in influencing CTL binding kinetics and function response primarily due to the different compositions at respective compartments. A LCMV mouse model will be used for this aim to study following infection leading to compartmentalization of antigen-specific T cells and how this reflects on the TCR/pMHC binding capability. It is hypothesized that CTLs at sites where LCMV replication is favored will exhibit higher 2D affinity than at other sites. More specifically, the 2D affinity of the CTL will vary transiently over the course of the viral and establishing homeostasis. For 2D kinetics, micropipette adhesion frequency assay will be conducted to measure the affinity. BFP will also be used to measure force-lifetime data and characterize the differences observed from different compartments. For functional study, intracellular cytokine staining assay from respective compartments will be performed and analyzed. This aim looks to understand how microenvironment influences T cell kinetics and its role in memory development. Various factors are known to negatively impact

CTL response and this could potentially mediate CTL binding kinetics and function. Using IV injection to tag adoptively transferred antigen-specific transgenic T cells, we can separate those from vasculature and from tissue-residence. The result of this will provide the dynamics that takes place over the course of the infection and as well, propose a mechanism of the regulation of T cell binding kinetics to obtain better understanding of how different compartments within SLO influence T cell development.

CHAPTER 2

BACKGROUND AND SIGNIFICANCE

2.1 Background

2.1.1 Cytotoxic T Lymphocytes

Immune response is branched into either innate or adaptive system and CTLs are a subset of leukocytes that are part of the adaptive system capable of inducing cytolytic activity on cells presenting foreign antigen peptide (p). TCRs expressed on $CD8^+$ T cells interacts with pMHC on antigen presenting cells, such as dendritic cells. Each T cell is unique in that they are specific in scanning pMHC complexes, which encodes antigens derived from pathogen and tumors [11]. The CD8 co-receptor on T cell surface potentiate the TCR-pMHC interaction by binding to the $\alpha 3$ domain of the MHC class I molecule, inducing a stronger signal [12].

Signaling of T cell activity by TCR/pMHC recognition is conducted by a group of transmembrane proteins, CD3 molecules, which form a complex with the TCR. Cytoplasmic domain of CD8 is associated with lymphocyte-specific protein tyrosine kinase (LCK) that phosphorylates immunoreceptor tyrosine-based motifs (ITAMs) found on the cytoplasmic segments of CD3. Followed by, recruitment and activation of Zeta-chain-associated protein kinase 70 (ZAP-70) in the cytosol takes place, which in turn phosphorylates linker for activation of T cells (LAT) and src-homology-2-domain-containing leukocyte protein of 76kDa (SLP-76), which results in signal amplification and diversification [12].

CTLs react to pathogen to clear infection within the host by priming, massive expansion, and differentiation that takes place in lymphoid organs upon interaction with

antigen presenting cells (APCs) with the outcome to protect the host with minimal local tissue damage [13, 14].

2.1.2 Antigen Presenting Cell

Antigens are toxins or foreign substances that induce immune response by the host either by TCR recognition or with antibodies. Antigens are composed of several antigenic determinants, known as epitopes, and these epitopes docked on MHC bind to a specific TCR. Viral entry into cell is by one of two pathways: (1) virions bind and fuse to the cell surface by the forming an interaction between glycoproteins on the virion and its respective proteins found on cell surface. (2) Alternatively, virions gain entry into cell by receptor-mediated endocytosis. The outcome of either of these pathways ensures the viral genome and associated proteins enter the cytoplasm [15-17].

Followed by the entry of the virus mediated through the endogenous pathway, virus associated proteins are degraded by the proteasome, which results in peptides that are shuttled into the endoplasmic reticulum. In the process, the complex pMHC is formed and is delivered to the cell surface, where antigen specific CD8+ T cells recognize and

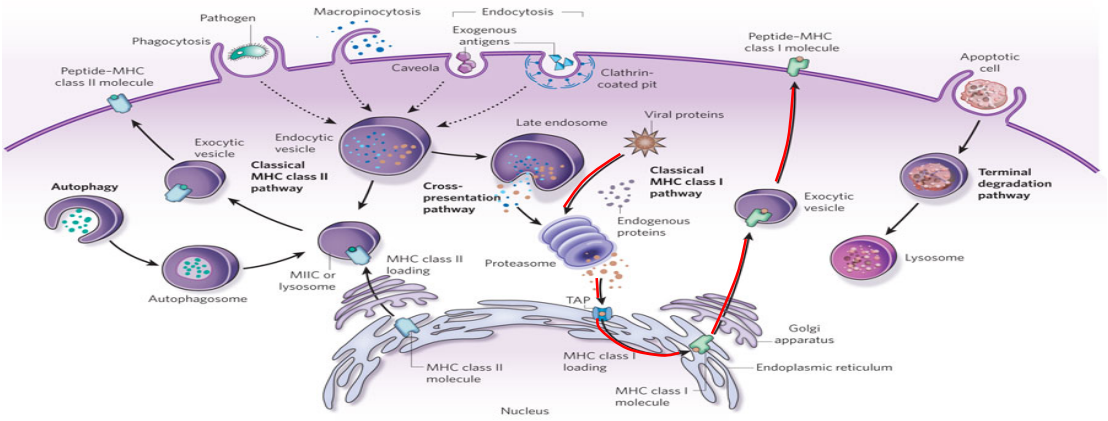

Figure 1. The endogenous pathway. The arrows highlighted in red depict the endogenous pathway. Intracellular pathogens are degraded by proteasome and the resulting peptides are shuttled into the endoplasmic reticulum and are complexed to the MHC molecule. The entire complex is then presented at the surface of the cell. Adapted and modified from [4].

act upon after forming interaction and initiate functional response mediated by recognition and potency of the peptide (**Figure 1**) [15-17].

2.1.3 Viruses

As humans carry lifelong, persistent viral infections, human CTLs are thought to play an important role in controlling these infections. CTLs recognize viral antigen in the form of HLA class I molecules, leading to activation of the CTLs to eliminate target infected cell through perforin/granyzme lytic granule secretion or killing mediated by Fas/FasL pathway to secrete antiviral cytokines [18]. Humans carry asymptomatic viral infection with more than 70% of adults infected with Epstein Barr Virus (EBV) and 80-90% of adult populations carry CMV [19, 20]. Other viral infection that are severe to the host are HCV (~170 million people worldwide) and Human Immunodeficiency Virus (HIV; ~33 million people worldwide) that poses challenge to the immune system with inhibitor molecules like the effect of programmed death 1 (PD-1) influence TCR activation has been observed [21-23]. However, another strategy by which virus evade immune function is via mutations that benefits its viral fitness [24]. Additionally, for successful replication and infection to other cells for survival, viruses inactivate cellular and organismal defense and tegument proteins found in the viruses disrupt antiviral immune system that includes, intrinsic, innate, and adaptive immune system [15].

2.1.4 Viral Immune Response

Chronic infection can severely disrupt the immune response capability of killing the target infected cell resulting incompetent of clearing the viral infection [25, 26]. At the onset of viral infection, normal viremia replication takes place due to delayed onset of CD4+ and CD8+ T-cell response, upon which transient control of viremia and rise in transaminases is observed. In chronic cases, some viral variants survive after the peak of the immune response and following the contraction of the CD4+ T cell response. Those

that survive, a select few based on viral fitness allows viremia to rebounds displaying persistent viral infection. At this point, if the immune system is incapable of adapting to the viral variants by inducing proper immune response to clear out the secondary viremia, a chronic infection is initiated and persisted for the host. Chronic infection in some infection is in part result of viruses bearing variant epitope representing a mechanism of persistence (**Figure 2**) [27].

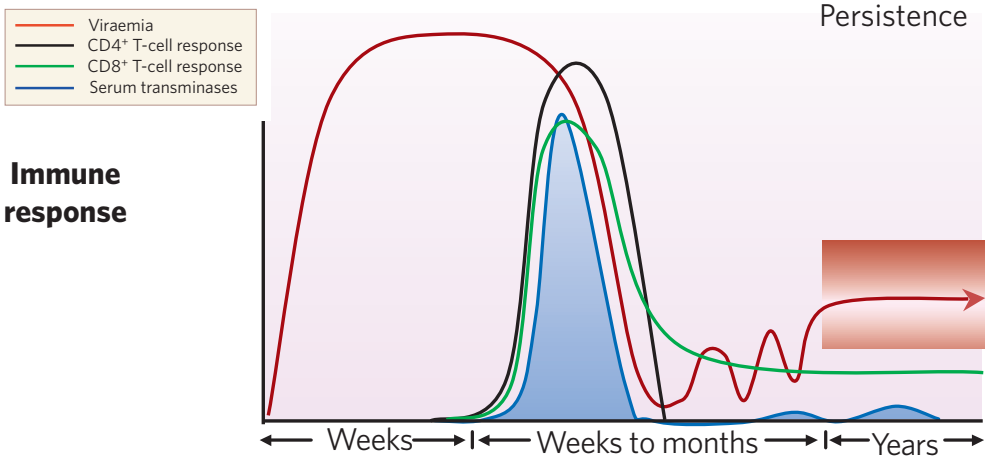

Figure 2. Schematic representation of the immune response during chronic infection. Persistent viral infection rebounds following cellular immune response due to many contributions (i.e., inhibitor molecules, exhaustion of T cells, and/or viral mutations). Adapted and modified from [6].

2.1.5 Viral Variant

The cause of TCR variants observed is a result of viral mutations. Typically, viral epitope specific TCRs on CTLs recognize highly conserved internal viral proteins. For the interest of this study, focus is on peptides associated with MHC class I molecules for its interaction with CTLs. While infected cell utilizes the machinery to express viral epitope on the cell surface, components of viral proteins from the virion can disrupt the presentation of the epitope by taking command of certain machinery and/or impact recognition of the TCR by generation of amino acid substitutions. One result of a single amino acid alteration can take place at anchoring residues resulting in complete loss of

epitope at the MHC groove, thus escaping immune response of this variant. Other results of single amino acid substitutions, when taken place at non-anchoring residues, leads to TCR residues to form loose interaction with the pMHC leading to an improper immune response to the target infected cell [10]. The latter strategy involving non-matching of TCR and pMHC specificity is a common mechanism of viral mutations observed in various viral infection, particularly in HCV [28, 29].

HCV genome is RNA encoded and it has been known to have a very high replication rate. However, the NS5B, an RNA-dependent RNA polymerase found in HCV virions, lacks proofreading function leading to various viral mutations potentially resulting in chronic infection [30]. The resulting mutations can contribute to different molecular mechanisms allowing escape from immune cell response. For example, the mutations of amino acid at MHC binding anchors attenuate binding of the entire peptide to the MHC molecule. Mutations at other hotspots can result in weak to even absence of TCR recognition. Primarily, viral mutations seen by any amino acid sequence alteration of the epitope that normally forms strong contact by the TCR residues, thereby preventing recognition or loose recognition of the epitope MHC class I complex by specific CTLs (**Figure 3**). This disruption leads to non-matching of the specificity of the TCR to the epitope and this common mechanism of viral mutations leading to its escape from immune cells is highly observed to that of chronic viral infection, particularly HCV [16].

However, T cells adapt to theses variations with their own capability of addressing such mutations, and one such example is at TCR specific to NP418-426 epitope of HLA-B*3501 in the case of an influenza viral infection [10]. TCR undergoing variations of such cases indicates signs of antigenic drift and emphasizes the ability to optimally recognize viral mutations to induce proper CTL response initiated by release of IFN-γ to block viral replication [31, 32]. Additionally, generated TCR variants has shown

to be compatible forming cross-reactivity against contemporary historical viral strains [33].

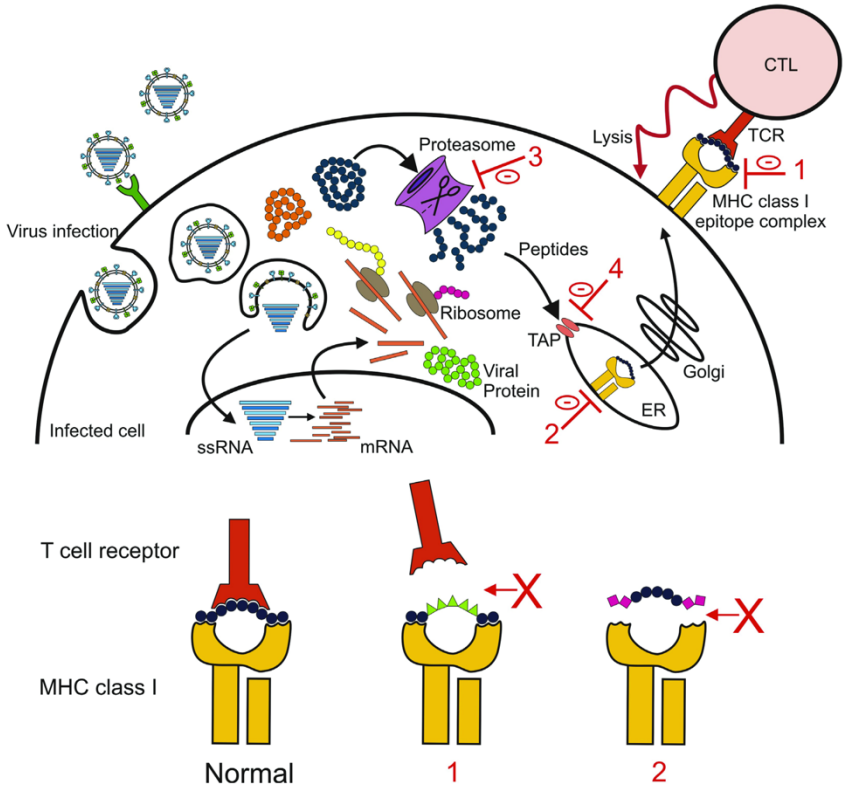

Figure 3. Viral epitope perturbation leading to ineffective CTL response. Mutations in viral epitope disrupting TCR contact residues leads to ineffective TCR recognition as shown in (1), or mutations of the anchoring residues of the epitope disrupts the affinity between the viral epitope and the MHC protein resulting in loss of a pMHC complex as shown in (2). In addition, viral tegument proteins can influence cellular machinery process to present viral epitopes on the surface and this can be achieved at steps involving proteasome and of transporter associated with antigen processing as shown in (3) and (4), respectively. Adapted from [10].

2.1.6 T cell development memory markers

Over the course of the viral immune response, naïve T cells undergo three phases following an antigen encounter: (1) expansion/activation, (2) contraction/death, and (3) memory/maintenance [34]. During the peak of the viral immune response, CTLs become heterogeneous both phenotypically and functionally. Early memory markers are classified as either short-lived effector cells (SLECs)or memory precursor effector cells (MPECs).

SLECs are high in abundance compared to that of MPECs during the peak of the immune response, but they quickly perish following viral clearance. MPECs plays a central role in developing into memory population (**Figure 4**) [8, 35, 36].

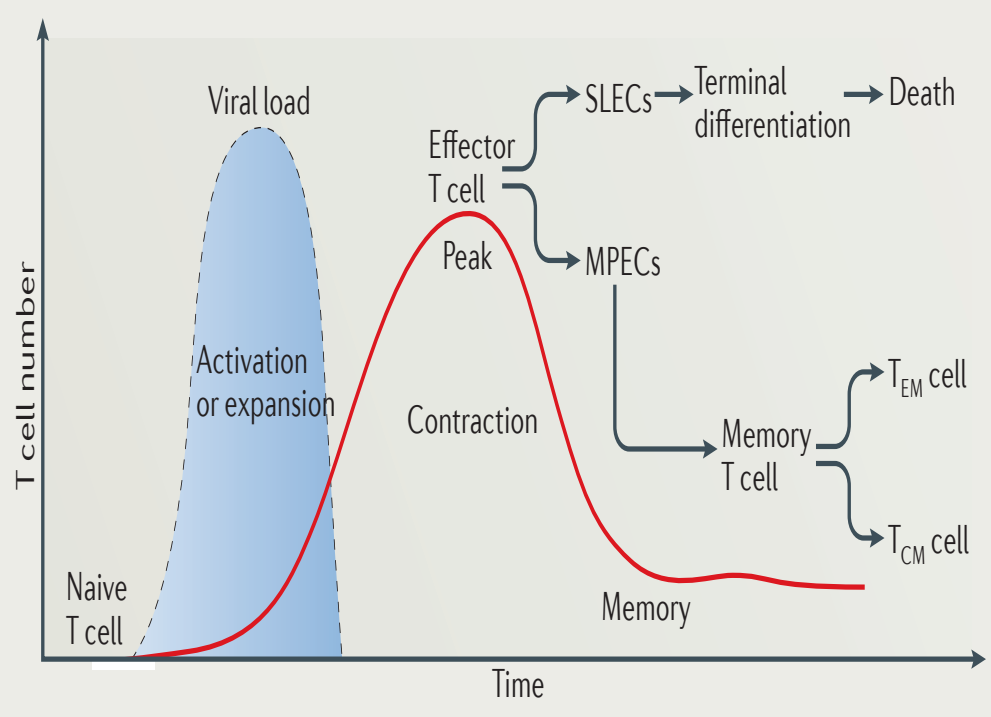

Figure 4. Schematic of CD8+ T cell immune response. Following viral infection, cognate CD8+ T cell develop into various subset both for short and long term homeostatic maintenance. Following expansion, T cell go through an early display of memory markers that sets precedent for the memory population and these distinct marker specific T cells exhibit different function. Adapted from [8].

2.1.7 Cytomegalovirus

Cytomegalovirus (CMV) is classified as a member of the *Betaherpesvirinae* sub-family of *Herpesviridae* and although the infection is persistent, it is asymptomatic. It infects 50-85% of adults by the age of 40 and virus has evolved to live in equilibrium with some cells and is typically in latent state of infection. However, immunocompromised individuals with CMV infection can lead to morbidity and mortality. The virus has a double-stranded DNA inside an icosahedral protein capsid.

Between the capsid and the outer lipid envelope contains proteinaceous tegument. The virus infects epithelial cells, B cells and monocytes [37].

The virus binds to the cell surface by forming an interaction between glycoproteins on the virion envelope and the heparin sulfate proteoglycans found on the cell surface. Followed by the fusion that takes place involving the envelope of the virion and the plasma membrane of the cell, the capsid and associated tegument proteins are released into the cytoplasm. The dynein inside the cytoplasm mediates the movement of these viral proteins to the nucleus allowing the double-stranded viral DNA enters the nucleus through the nuclear pore [15, 38]. The viral genomic DNA is encapsulated inside an icosahedral protein capsid and between this capsid and the outer lipid envelope contains proteinaceous tegument. Some of these tegument proteins are responsible for modulating the infected cell that disrupts the immune response during viral immune response of the host. The most abundant tegument protein, phosphoprotein 65 (pp65), is responsible for modulating the host cell immune response during CMV infection (**Fig. 2**). As importantly, it also serves as the immunodominant antigen for CD8+ T cells and the epitope that is most prevalent of this antigen is NLVPMVATV peptide [15].

2.1.8 Lymphocytic choriomeningitis virus

Lymphocytic choriomeningitis virus (LCMV) carries RNA as its genome that gains entry into cell by binding the glycoprotein of virion to the α-dystroglycan found on the cell surface [39]. LCMV is a common pathogen for house mice, but humans can be infected as well and this common pathogen causes inflammation in the meninges lining the brain and spinal cord [33]. Two common strains of LCMV are Armstrong (acute) and Clone 13 (chronic) that are widely used to study in mice to understand viral infection progression and how that influences immune response. The most prominent peptide used for this model is glycoprotein 33 (gp33) [39]. The Armstrong infection elicits a unique kinetics different from the chronic strain, Clone 13 and alongside elicits an immune

response composed of diversified clones of cognate specific T cells recognizing various portions of the virus. When naïve CD8+ T cell interacts with its cognate antigen, an induced T cell immune response is initiated that can be divided into three phases involving (1) activation and expansion of cognate populations, and after the peak of the response (7-8 dpi), (2) contraction of the expanded population begins, and (3) the surviving populations contribute to the maintenance for the memory population (**Figure 6**) [9, 34, 40, 41].

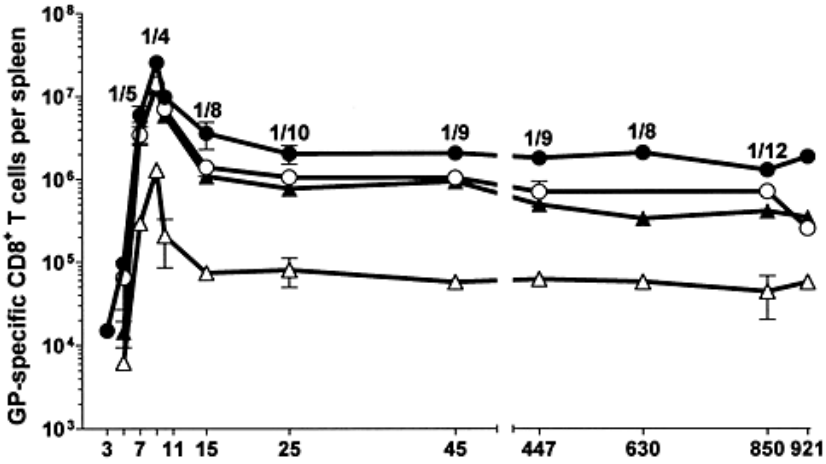

Figure 5. Various epitope-specific CD8$^+$ T cell clones from activation into memory phase of the immune response. Total numbers of GP_{33}- (●), GP_{118}- (○), GP_{276}- (▲) and GP_{92}- (△) specific CD8$^+$ T cells per spleen. Adapted from [9].

2.1.9 Spleen

Lymphoid organs play a central role in facilitating the lymphatic system, which maintains host fluid balance, transportation, and works along the immune system. Sites associated with accumulations of lymphoid cells are coined primary and secondary lymphoid organs (SLOs). Primary lymphoid organs generate functionally mature naïve lymphocytes in the absence of foreign antigens, whereas SLOs are sites that responds to foreign antigen invaders [42]. SLOs initiate the adaptive immune responses, in which APCs, such as dendritic cells and macrophages, capture pathogens and bring these APCs in close contact with cognate lymphocytes. This interaction provides a niche for

differentiation to take place for the immune cells within the host to limit the spread of the infections (**Figure 6**) [43]. The spleen, being the largest SLO, plays an essential function to counteract against circulating antigens. Spleen is compartmentalized distinctly into two compartments: WP and RP. Blood enters the spleen carrying antigens and other components and macrophages that reside in WP at the marginal sinus capture these pathogens. Blood components continue to travel through the marginal zone in a direction away from the WP regions into the RP to return to the vasculature network via venous sinuses [44].

The function of leukocytes in the spleen, depending on the localization, conduct discretely. RP macrophages phagocytose aging RBCs and regulate iron recycling and release, whereas marginal zone macrophages utilize patter-recognition receptors to remove a subset of bacteria and viruses. Residents at marginal zone, like B cells and dendritic cells, along with the macrophages, also uptake antigens and migrate to WP for antigen presentation. Entrance to WP is restricted to a subset of cells (B cells, dendritic

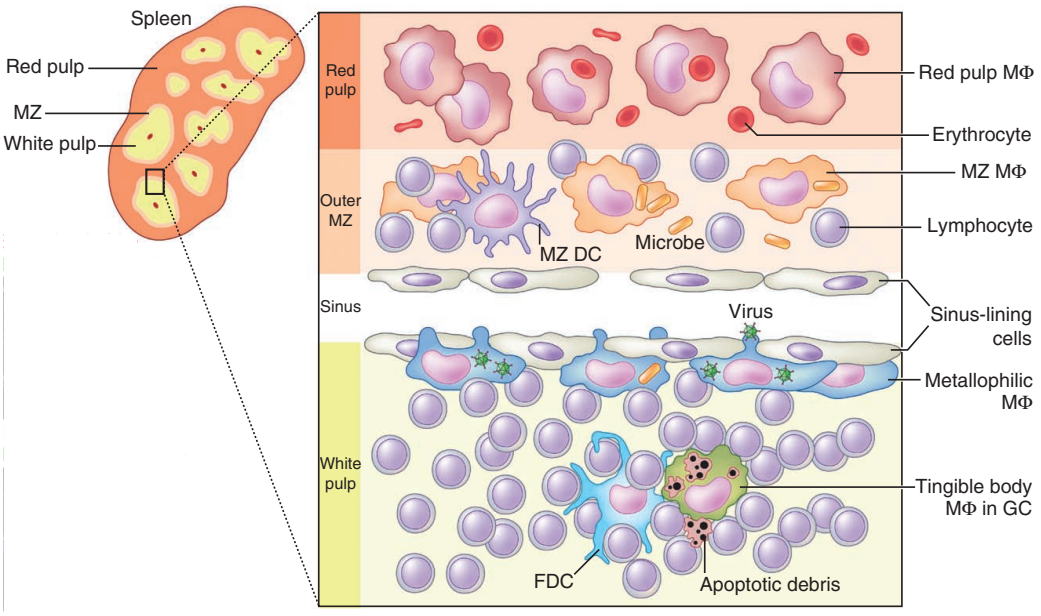

Figure 6. Mouse spleen microanatomy depicting WP and RP and its localization of its residents. WP and RP are functionally and morphologically distinct compartments. WP contain a wider variation of cellular populations (i.e., $CD4^+$ and APCs) in comparison to RP. Adapted from [7].

cells, CD4+ and CD8+ T cells) and components exit out of spleen mostly via splenic vein in the RP, however some cells from WP exit via a local network of efferent lymphatic vessels that connects to the other parts of the host [45].

2.2 Significance

T cell activation and priming is an important feature of the immune response of the host to effectively clear viral pathogen and establish homeostasis. Particularly, interest in characterizing the dynamic changes of the TCR binding kinetics influenced by organ structures and as result, the impact ligand recognition is highlighted in this study. This study also aims to elucidate the mechanism driving the effects on TCR-pMHC kinetics both by *in-vivo* and *in-vitro* conditioning. Viral infection to the host also poses problems that stem from viral mutations, which occurs to increase viral fitness by evading immune responses. The potency of these viral mutations binding is typically determined by lysis response assays and the affinity or avidity measurements of the mutated pMHC to the host sample. However, the measurements are provided using 3D assays, thereby not even proximally mimicking the natural interaction that takes place within the host. This study also aims to investigate the kinetic parameters mimicking natural interaction setting (as in utilizing the full cell) by characterizing affinity and correlating the findings with functional assay. More importantly, the contribution of force on bond-lifetime is highlighted in the context of viral mutants with the capability to lower cytolytic responses of CTLs. The resulting insights of this study provides evidences to understand how to optimize interaction with viral variants to effectively trigger cytolytic function on how to improve vaccine and through emerging technologies, such as, chimeric antigen receptors. Overall, this study will contribute to describe how viral epitopes and leukocyte interaction impact on recognition or tolerance upon infection using binding kinetics providing a unique perspective to the field of immunoengineering.

CHAPTER 3

MATERIALS AND METHODS

3.1 Reagents

3.1.1 Proteins

For the LCMV and CMV study, we used synthesized recombinant peptides from Genemed Synthesis Inc. and pMHC monomers were developed by the National Institutes of Health Tetramer Core Facility at Emory University. For LCMV study, the peptide sequences were glycoprotein (gp33) (KAVYNFATM), gp35A/V35A (KAAYNFATM), and gp276 (SGVENPGGYCL) bound to H-2Db or a mutant H-2Db (the α3 domain in mouse H-2Db is replaced with the α3 domain of human HLA-A2) [46, 47]. For CMV study, the peptide sequences were CMV pp65 NLV (NLVPMVATV), T8V (NLVPMVAVV), and M5I (NLVPIVATV) bound to HLA- A*02:01 or a mutant HLA-A*02:01 (the heavy chain of D227K/T228A in the α3 domain of HLA-A*02:01 that appear to be important for the interaction with CD8) [48-50]. All these pMHC monomers are biotinylated on the C-terminus. Biotinylated anti-TCR was used to determine the adhesion frequency and 2D affinity to P14 TCR on P14 T cells.

For the LCMV study, CD4 ablation was proceeded by intraperitoneal administration of CD4-depleting antibody (GK1.5, 500 μg/mouse) at 1 day before infection and 0 dpi on C57BL/6 [51-54]. As for FoxP3-DTR mice, $FoxP3^+$ Treg was depleted by intraperitoneal administration of diphtheria toxin (1 μg/mouse) at 7, 8, and 10dpi. As for inhibiting the effect of TGF-β signaling, C57BL/6 mice were treated with TGF-β inhibitor (SB431542, 20 mg/KG•mouse) intraperitoneally at 8, 9, and 10 dpi.

Lipid raft disruption was performed *in-vitro* through two means: sequestration and depletion of cholesterol. Cholesterol sequestration on splenocytes was performed by 30 min incubation of nystatin (25 μg/mL) at 37 °C prior to Fluorescence activated cell sorting (FACS) cells, whereas cholesterol depletion was performed by incubating splenocytes with cholesterol oxidase (5 U/mL) for 30 min at 37 °C prior to sorting cells. Unlike nystatin treatment, cholesterol oxidase was present during micropipette assay.

3.1.2 Protein coating on RBC surface

Purification of human RBCs from peripheral blood of healthy donors at Georgia Institute of Technology with protocol approved from Institute Review Board [55-57]. Purified RBCs were biotinylated with various concentrations of Biotin-X-NHS (EMD) and stored in Experimental additive solutions 45 (EAS-45) buffer over a period of 4-6 weeks. To link biotinylated proteins on RBCs, biotinylated RBCs were initially incubated with streptavidin at 1mg/ml final concentration in room temperature (RT) for 20 mins. After incubation period, excess unbound streptavidin is washed off by washing three times, after which streptavidin coated-biotinylated RBC is incubated with the biotinylated protein (pMHC or antibodies) for an additional 20 min at RT, followed by washing similar to washing off excess streptavidin.

3.1.3 Site density measurements

Biotinylated proteins on RBCs were determined by flow cytometry to obtain the 2D effective affinity [55-57]. PE-conjugated monoclonal primary antibodies or secondary antibodies were stained on RBCs to measure site densities of pMHCs or anti-TCR and T cells for CD8 or TCR site densities. The measured MFI for each sample measured is converted to the number of molecules per surface area (μm^2) based on PE calibration beads with known number of PE molecules. As T cells undergo change in size during the

course of the infection, the size of T cell was measured for every 2D micropipette experiment. However, RBC size was kept constant for all experiment.

3.2 Assays

3.2.1 Animal and cell for LCMV study

For understanding the role of spleen compartmentalization, P14 TCR transgenic, C57BL/6 and FoxP3 DTR mice were utilized and housed at Yerkes National Primate Research center at Emory University according to institutional approved protocol by Institutional Animal Care and Use Committee. P14 TCR recognize gp33 epitope of LCMV Armstrong clone. Transgenic P14 CD8+ T cells were adoptively transferred to either C57BL/6 or FoxP3 DTR mice and was infected with LCMV Armstrong intraperitoneally with 2×10^5 plaque-forming unit. Adoptively transferred transgenic P14 T cells display specific markers not endogenously present within the adoptively transferred host allowing cells to be tracked once transferred. Several days following infection, fluorophore-conjugated antibody against Thy1.1$^+$ or CD45.1$^+$ is intravenously (i.v.) injected to the host (3 μg/mouse) to tag P14 T cells in vasculature and after few minutes, the host is sacrificed 3 min after antibody injection to prevent staining of P14 T cells embedded within tissue such as WP. Harvested spleens were then stained *ex-vivo* using antibody against Thy1.1 or CD45.1 with a different fluorophore conjugated from the i.v. injected. Using BD FACSAria^{TM}, stained P14 samples were sorted from splenic RP (i.v. and *ex-vivo* double positive) and splenic WP (i.v. negative, *ex-vivo* positive) (**Figure 7**). Furthermore, additional antibodies were stained for memory markers following spleen harvest with KLRG-1^{high}/CD127^{low} expressing cells categorized as SLECs and cells expressing KLRG-1^{low}/CD127^{high} as MPECs. Sorted cells were washed and stored in PBS with 2%FBS in 4 °C for use up to 24hrs.

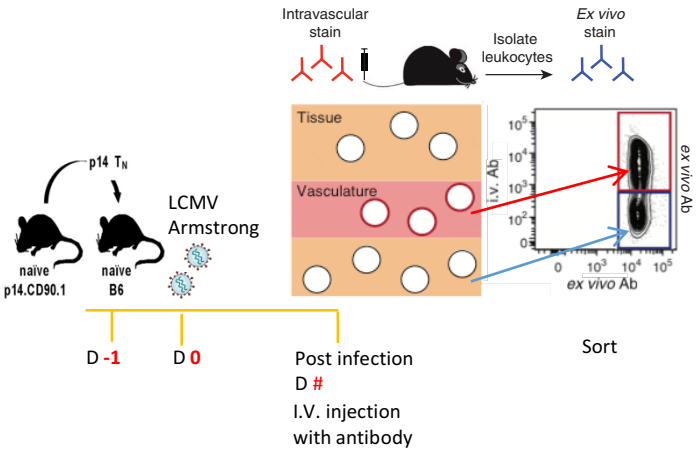

Figure 7. Experimental scheme for adoptive transfer. P14 T cells were adoptively transferred into B6 mice one day before infection with LCMV-Arm and isolated on indicated dpi from WP or RP. Prior to sacrificing mice, fluorophore conjugated antibody targeting transgenic markers on adoptively transferred P14 cells by intravascular staining. An ex-vivo antibody with a different fluorophore is added to the spleen sample after mouse is sacrificed. The sample is gated of the two contours and then sorted, respectively. Adapted and modified from [3].

3.2.2 CMV positive-specific T cells by *in vitro* enrichment from PBMCs

Peripheral blood mononuclear cells (PBMC) of CMV positive HLA-A2^{+}donors were isolated and incubated with 10 μg/ml NLV peptide in primary culture. Cells were maintained by the addition of 50 U/ml human recombinant IL-2 every 2-3 days. After 2-3 weeks of culture, a polyclonal enriched peptide-specific CTL lines from each donor was established and cells were stained with NLV-tetramer to validate increased frequency of NLV-specific population. For conducting 2D biophysical experiments and DNA force probe experiment, the enriched samples were stained with antibodies against CD3 and CD8 using different fluorophores to obtain a higher degree of purified NLV-specific population. Briefly, a small portion of the PBMC with antibodies against CD3 and CD8 was aliquoted to another tube and was stained additionally with NLV-tetramer conjugated with a different fluorophore. This sample was initially run to determine the frequency of NLV-specific CD8+ T cells. As PBMCs originally pulsed with NLV

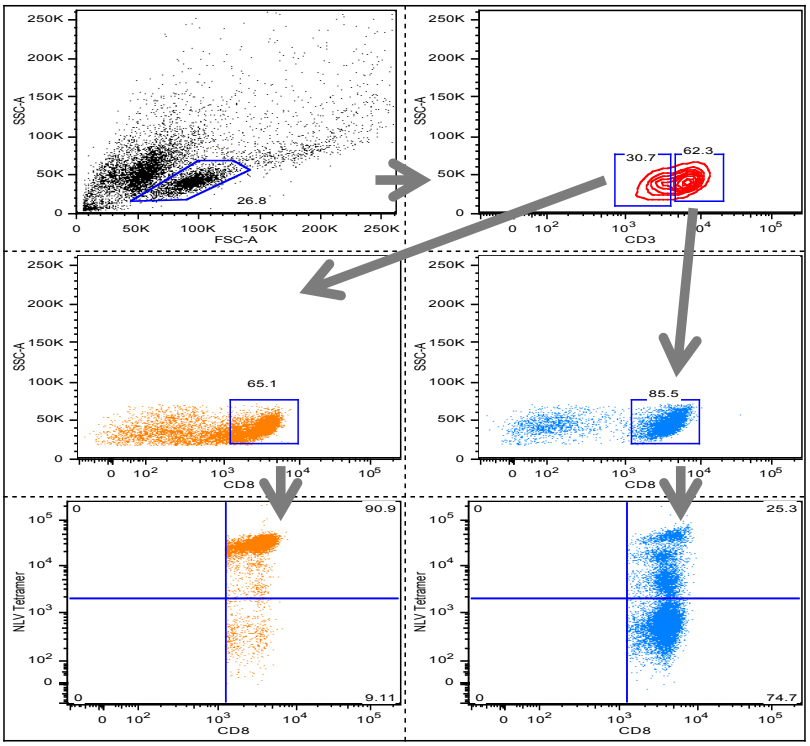

Figure 8. NLV tetramer frequency of CD3 population. Gating was set for lymphocytes, $CD3^{low/high}$ and $CD8^{high}$. Grey arrows direct the pathway moving from one panel to the other. This template was used to do sorting of cells stained with CD3 and CD8 for various assays.

peptide resulted in a subpopulation of cells at various stages of activation, the more activated state has been correlated with downregulated CD3 expression. This along with high CD8 expression correlated with high frequency of NLV-specific T cells stemming from the tetramer staining (**Figure 8**). This $CD3^{low}/CD8^{high}$ template was used to determine the percentage of $CD3^{low}$ population and this percentage value was used an initial value that was further lowered for the enriched PBMC sample containing antibodies-alone. The enriched PBMC sample containing antibodies-alone was primarily used to sort enriched NLV-specific T cells from the whole mixture. A lower $CD3^{low}$ percentage was set for the sorted sample primarily due to the absence of the third fluorescence (tetramer) in the sample, and thereby, ensuring increased purity of NLV-specific T cells to conduct 2D biophysical assay and functional studies. All samples were

stained at 4°C and in rotation for 30 min to primarily lower the activation through CD3 antibody. Following sorting, cells were washed and stored in PBS with 2%FBS in 4 °C for use up to 24hrs.

3.2.2 2D micropipette adhesion frequency assay

A customized inverted microscope (TMD Diaphot, Nikon) objective lens with two 3D micromanipulators (Newport) facing each other that holds capillary glass pipettes that was pulled (Sutter Instruments) and shaped using an in-house built forge. The pipettes are inserted into a chamber that contains L-15 media medium (Sigma-Aldrich) plus 5mM HEPES and 1% bovine serum albumin (BSA). The pipettes were connected to a home-made manometer system allowing negative pressure to aspirate and hold cells at the tip of the pipettes. Prior to applying suction pressure, pipettes were mounted on the manipulators and an individual RBC and T cell were aspirated, respectively and positioned facing each other (**Figure 9**). Using a piezo actuator controller, the aspirated RBC comes into contact with the T cell for a duration set by the user and then the RBC aspirated pipette is retracted using LabView software (National Instruments) and DAQ 6008 (National Instruments). Using a CCD camera (MTI DC330, Dage), one of the two events were observed every cycle: (1) adhesion or (2) no adhesion. When the RBC is being retracted after contact and no elongation of the RBC is observed at the point of contact, then this particular cycle is categorized as an event where no adhesion has taken place. However, if during the retraction phase the RBC elongates and deforms prior to complete detachment from the cell, then this particular cycle is categorized as an adhesion event. The frequency of adhesion event (P_a) between the RBC/T cell pair contact is observed for 30 cycles.

By increasing the contact time (t_c), an adhesion frequency curve is generated and along with the receptor/ligand densities, the data generated is fit using a nonlinear

regression to with least mean square method to the following probabilistic kinetic equation for a single-step monovalent receptor ligand interaction:

$$P_a = 1 - \exp\{-m_r m_l A_c K_a [1 - \exp(-k_{off} t_c)]\} \quad (1)$$

Two parameters are derived from the following equation using Excel solver: (1) zero-force off-rate k_{off} (s^{-1}) and (2) the 2D effective binding affinity, $A_c K_a$ (μm^4). The 2D effective affinity consists of two combined parameters, where K_a represents the 2D affinity and the A_c denotes the consistent contact area formed between the RBC and the T cell during impingement.

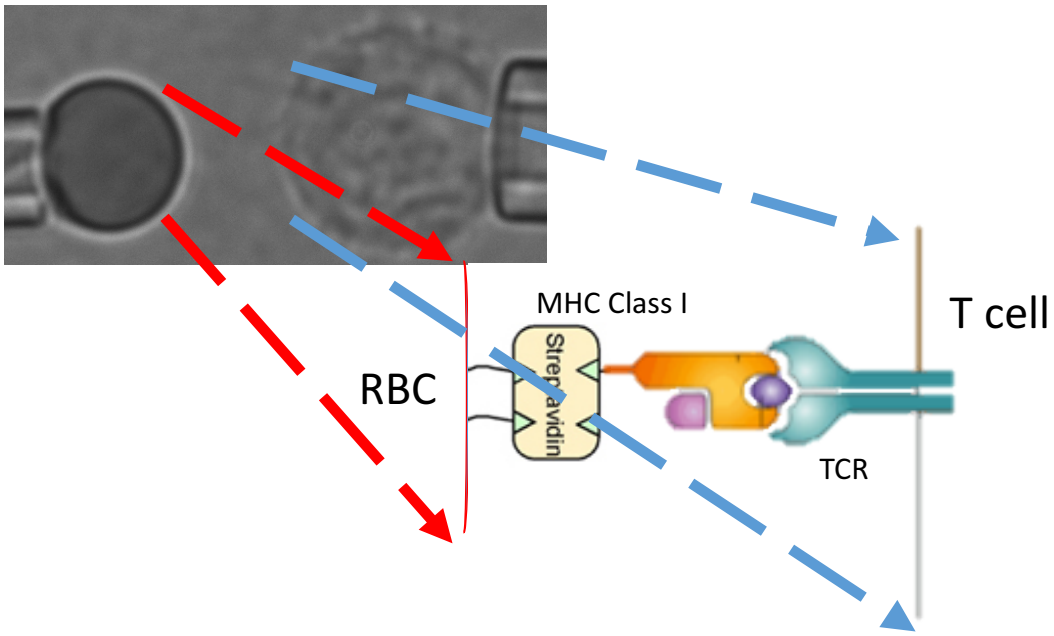

Figure 9. Micropipette adhesion frequency. RBCs coated with protein of interest is aspirated to one side of the pipette and the apposing pipette aspirates a leukocyte prior to contact. Biotinylated proteins are bound covalently to RBC by streptavidin. For the adhesion frequency assay, impinging apposing cells to form a contact and maintain for a certain duration and during retraction, the user visualizes if an elongation takes place to see if an adhesion even takes place.

For experiments where the primary objective is to measure the 2D effective affinity, the contact time is kept constant and the binding frequency is measured. This t_c is set by first measuring the binding frequency at various t_c and observing when the t_c

approaches steady state, which will be termed t_{st}. This allows equation 1 to be log transformed and simplify the equation into the following:

$$A_c K_a = \frac{-\ln [1-P_a(t_{st})]}{m_r m_l} \quad (2)$$

For measurements of tri-molecular interaction between TCR-pMHC-CD8 binding, the right hand side of equation 2 represents the average number of bonds <*n*> (the numerator) per unit densities of TCR and/or pMHC.

For the LCMV study, t_{st} was set at 4 sec and for the CMV study, t_{st} was set at 2 sec. The respective t_{st} for each system reached steady state in regards to the adhesion frequency. They were not the lowest t_c to reach saturation.

To understand the level of non-specific adhesion that can stem from this technique, RBCs coated with streptavidin or with self-A2 HLA-A*02:01 was used to address non-specific binding. Binding frequency were less than 3% for biotin with streptavidin and also for RBCs with self-A2 HLA-A*02:01.

3.2.3 Thermal fluctuation assay

In order to obtain k_{off} by performing thermal fluctuation assay, force clamp was set at low force (1pN) and a softer spring constant was set (0.25pN/nm) to obtain lifetime measurements. With the nystatin treated RBC acting as a soft spring constant and given the BFP's high resolution, a more accurate measurement of the k_{off} is obtained than the k_{off} obtained through 2D micropipette adhesion frequency assay.

Lifetime is measured for BFP [58, 59] using RBC that act as a force transducer. The nystatin treatment to RBC is a hypotonic treatment allowing RBC to swelling. The RBCs were biotinylated allowing streptavidin coated beads linked to biotinylated proteins to be placed on the RBC (**Figure 10**). The RBC is captured and held by a borosilicate micropipette termed probe pipette with controlled aspiration pressure. The streptavidin coated bead aspirated by the bead pipette allows the user to place the bead on the apex of the RBC. Based on the diameter of the pipette, the diameter of the RBC, and the length of

the interface between the RBC and the bead at the apex of the RBC is measured. These parameters determine the distance of the manometer to be placed to apply the negative pressure to set the spring constant of the RBC at 0.25-3 pN/nm. A third pipette termed target pipette has the cell aspirated and is faced apposing the target pipette. The target pipette is controlled by a piezo actuator allowing contact to be made with the bead.

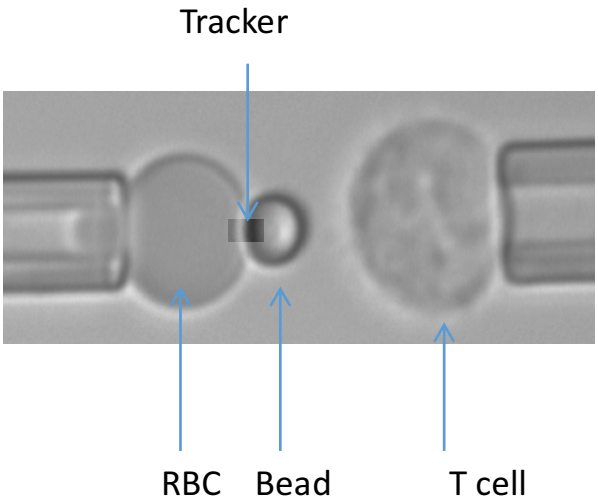

Figure 10. Biomembrane Force probe assay. Video-micrograph of a BFP with an RBC ligand-coated bead reporter held facing a T cell aspirated to an apposing pipette. A swollen RBC is aspirated with a ligand coated bead that is mounted to the RBC apex. T cell bearing pipette is the target that is mounted to a computer-controlled piezo translator apposing bead mounted RBC. A tracker is placed at the interface of the bead and the RBC.

A high speed CCD camera with frame rate of 1,500 frames/s captures the greyscale profile of the interface of the edge between the RBC and bead complex. This allows to track the axial displacement of this profile following impingement and following retraction. Lifetime detection is described in detail in the force-clamp assay section. By converting the exponential component by taking the natural log results in the plotting the survival probability curve (natural log of the number of events at the specified lifetime).

3.2.4 Force-clamp assay

Following interaction with ligands, anchoring receptors must withstand mechanical forces projected by the environment (i.e. external fluid flow and tissue or substrate stresses) and by the internal cytoskeletal tension from receptor and ligand anchoring cells. Therefore, initially we wanted to understand how receptor-ligand interactions is influenced under force.

Conventional methodology of force measurement composes of atomic force microscopy, optical tweezers, and BFP to understand the effect of force on bond interaction at a single bond level and ideally, in these experiments, surfaces are coated with either the receptor or the ligand to have them interact with their complement protein and the kinetic parameter is measured at the force.

Using the BFP, force is loaded to a constant level and held until the bond breaks. If the average bond lifetime decreases as the force increases, the bond exhibits slip bond, presumably because force pulls out the ligand. However, as the average bond lifetime increases with increasing force up to a critical force, the interaction exhibits a catch bond and this region is called the catch regime. Above the critical force, even catch bonds enter

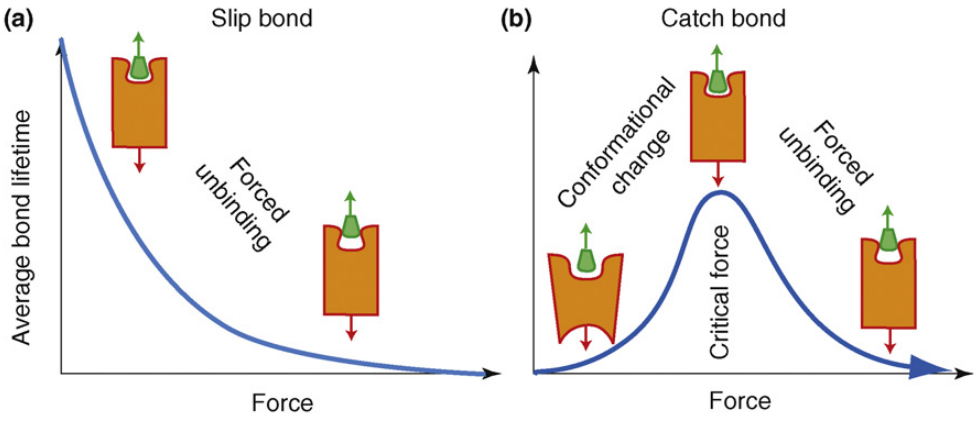

Figure 11. Bond mechanics. In the absence of mechanical activation, the protein-protein interaction exhibit slip behavior as seen in (a), where the increase in force decreases bond lifetime. However, in the presence of mechanical activation, conformational change can lead to increase bond lifetime until reaching critical force as seen in (b). Further increase in force following critical force leads to a slip behavior. Adapted from [5].

a slip regime where force shortens lifetime, presumably because further force overpowers the activated bonds **(Figure 11)** [5].

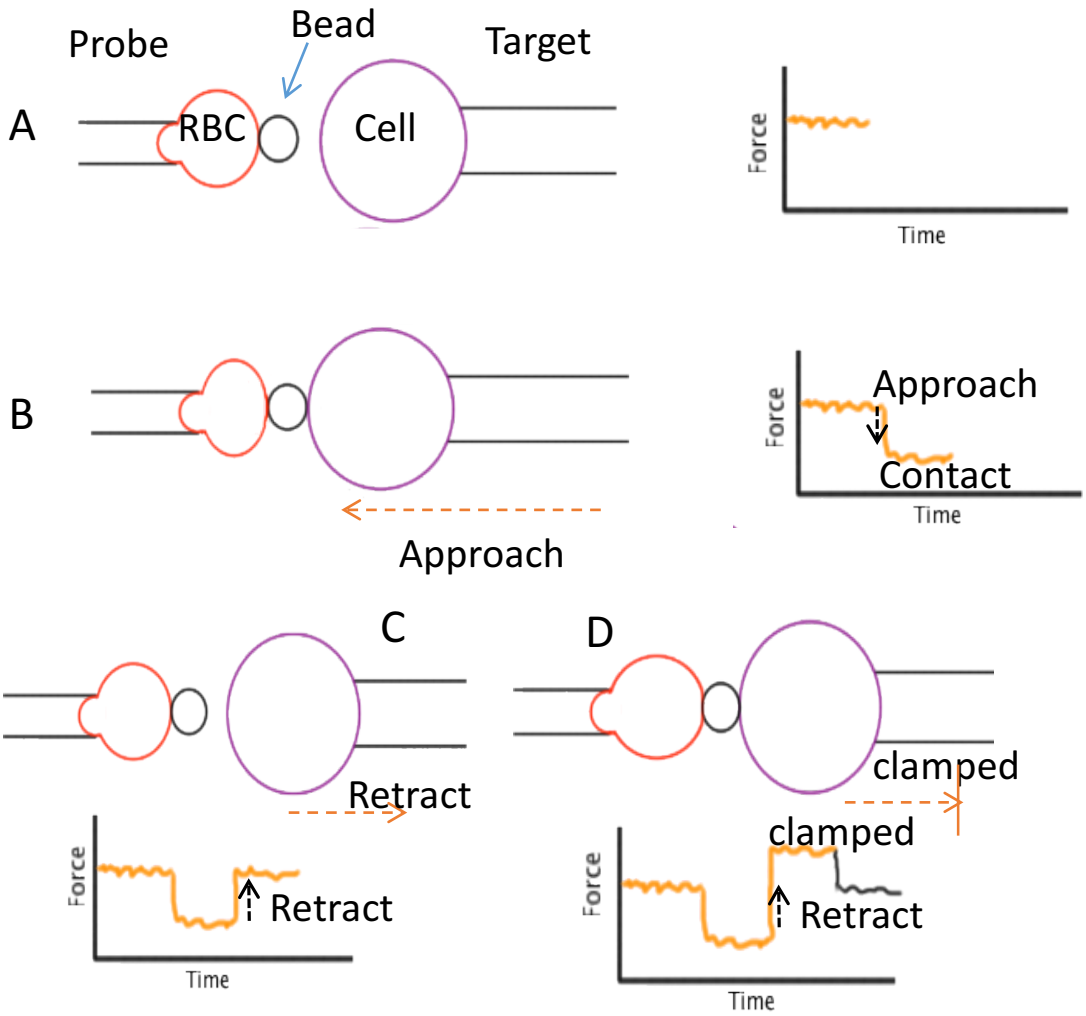

Figure 12. Force-clamp assay. T cell approached the bead to make an initial contact and was retracted to observe one of two things: (1) no adhesion, in which the signal leveled off to the point prior to the contact or (2) adhesion and clamped, in which the signal clamped to the set force and lifetime was recorded.

A Nikon inverted microscope (TiE) with 40X/0.75 objective lens and mounted with three micromanipulators: two pipettes (target and probe pipette) are opposing each other and one diagonally positioned facing the probe pipette.

For the force-clamp assay, repeated cycles to measure lifetime under a specified force is performed. Each cycle is composed of the following: (1) the target cell/bead

approaches using the piezo actuator and impinges at a certain force (5-40 pN) on the bead adhered to the apex of the nystatin treated RBC, (2) the target cell/bead stays in contact for a set time period (0.1-2 sec) and is then retracted in which one of the two events takes place. A bond is not formed between the receptor and the ligand, resulting in the target cell/bead pipette to reset to its original position to begin the next cycle or a bond is detected at the force clamped signified by a tensile force, in which the lifetime is recorded until the survival of the bond ruptures (**Figure 12**). In some cases, adhesion takes place at set force, however, a stable lifetime does not prolong and stabilize, in which this particular profile is not considered for analysis. For the force-clamp assay, the RBC spring constant is set to 0.3 pN/nm and retraction speed set at 3 μm/s with loading rate 1000 pN/s. The entire cycle was repeated for 200 cycles and the binding frequency was kept at 20% binding frequency to ensure single pair of receptor-ligand interaction taking place. The force range used varied from 5 to 40 pN and lifetime data spread was binned 3 to 6 points to describe the bond-lifetime behavior. This was the sample mean for each bin and additionally, bootstrap method was performed to identify the magnitude of the fluctuations. Briefly, repeated samples are drawn (of the same size with replacement) from the data set at a large number of times providing a sample distribution from these repeated samples.

3.2.5 Calcium Cell trap

Using soft lithography, microfluidic cell trap devices were fabricated. Briefly, negative molds were initially fabricated using UV photolithographic process and patterned wafers were treated with T2492 vapor to prevent PDMS adhesion prior to the molding process. After adding PDMS to the mold and cured, molded PDMS was peeled and devices were used for experiments. For fluidic flow, medical grade polyethylene tubings were used and holes for these tubings were punched to fit 19 gauge needles. To

place the PDMS on an inverted microscope, the PDMS was bonded to a cover slip glass [60, 61].

3.2.6 Cell trap preparation

Tubings connecting the outlet of the device was initially washed the inner tubing with sterile PBS. The microfluidic device was primed using the PBS and the device was checked under a microscope for any bubbles. Following thorough inspection of the device of the presence of any bubbles, 10 µl of biotin BSA was added through the inlet using 10 µl pipette tip. Flow into the device was accomplished by the pressure difference created by gravity from the placement of the tubing connected to the outlet. Device was washed with PBS and subsequently incubated with streptavidin similar to the step of

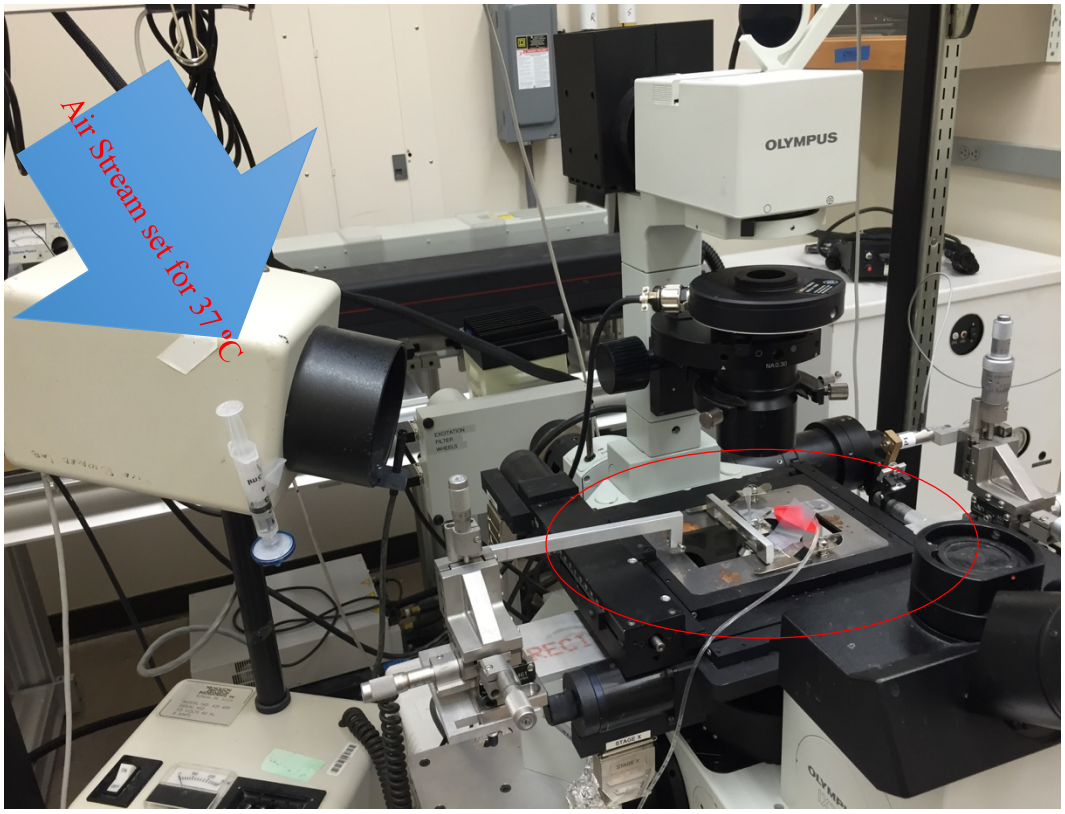

Figure 13. Fluorescence cell-trap setup. Microfluidic cell trap placed at the microscope stage shown in red oval and placed nearby an air stream to maintain temperature at 37 ºC.

biotin BSA. The last step of functionalizing the device was done by incubating with the biotinylated protein of interest.

Fluo-3 was incubated with the cells to detect calcium flux. After washing, upon which cells were loaded into the device and the device was positioned on the microscope stage. All experiments were performed under a temperature controlled environment (37°C) (**Figure 13**).

3.2.7 Data Collection and Analysis from cell trap device

Fluorescence microscopy was performed using a confocal microscope. Using Micro-Manager, an open source microscopy software, image acquisition with combination of time-lapse, multi-channel imaging, and z-stacks provided the experiment to be conducted following the events of the first cell viewed in the region of interest (ROI) and trapping [62]. Images from portion of the device over the duration of the experiment was sequentially captured. Custom Matlab® (MathWorks) GUI from Two-Photon processor and SeNeCa [63] were modified to fit the experimental objectives for image processing. The entire process of user modification was minimized to provide consistency, reproducibility, and robustness by further modification done by the author of this dissertation.

Briefly, images were cropped to reduce computational resources from the processing to contain only the portion of cell trapping of interest using ImageJ. The images captured displayed to have an uneven illumination from the light source. Therefore, as a first step towards analyzing, background correction to normalize the light intensity from the microscope across the image was performed. By varying multiple parameters, a mask is established for all the cells on the image of the traps. For each sequence of the image, the mask is established with individual cells labeled. Due to the cell mobility over the duration of the experiment, an additional parameter was set to track the cell from each image to ensure continuous observance of the fluorescence reading.

The program also has parameters to help discriminate single vs. multiple cells to ensure proper data collection. The objective of this method is to collect single cell calcium flux response by collecting the mean intensity of each ROI over time. Additionally, manual visualization of anomalies that the program accounts for were removed from the analysis. The normalized intensity for each object was determined by the ratio difference of the intensity after settling to the surface to the initial intensity at the point of contact on the surface of the trap.

3.2.8 DNA Force Probe

Custom synthesized oligonucleotides purified by Integrated DNA Technologies consisted of ssDNA hairpin hybridized through two 21-mer DNA handles to ligand and anchor strands. The ssDNA for solid support attachment on coverslips by commonly used chemistries. More specifically, modifications for oligonucleotide attachment was done by modifying 3' amine-modified oligonucleotides covalently linked to succinimidyl glutaramide (SGA). The SGA is part of the maleimide-PEG-SGA linker, where the maleimide is reacted with the sulfhydryl of the 3-mercaptopropyl-trimethoxysilane (MPS) on the glass coverslip MPS coated surface. Maleimide-PEG-SGA forms a thioester bond that is covalently linked on the MPS surface of the coverslip. The 5' end is modified with a biotin group to link biotinylated proteins by linking divalent streptavidin between the protein and the DNA force probe. The multiplexed tension probe surfaces on the coverslips were generated by having each hairpin sensor folded separately and then mixed with linker at various ratios followed by adding them to the MPS surface for overnight incubation [2, 64].

Following preparation of the functionalized coverslips, cells are added to the surface and allowed time to settle down to the surface (~5 mins) before conducting fluorescence microscopy.

The hairpin of the ssDNA contains a fluorescence resonance energy transfer (FRET) pair that consists of a quencher (acceptor) and a Cy5-QSY21(donor), which provided superior quenching efficiency. Live cells were imaged in 1X PBS at room temperature. For imaging, Zeiss LSM 710 NLO confocal microscope was used using a plan-apochromat 63X/1.4 oil immersion objective lens. The microscope was driven by the Zeiss Zen 2012 microscope and imaging software package, with the system including a fully automated precision stage, definite focus module without loss of focus. The LSM 710 is equipped with a red 633 nm helium-neon laser for continuous spectral detection for detection and excitation of Cy5 fluorescence intensity, which closely matched dye configuration of Alexa Fluor 647 in the system. As Cy5 dye conjugated to the oligonucleotide strand is utilized in this study, cells initially sorted of anti-CD3 (clone UCHT1) conjugated to FITC and anti-CD8 (clone HIT8a) conjugated to PerCP-Cy5.5 provided strong spectral overlap between PerCP-Cy5.5 and Cy5 dye. Therefore, anti-CD8 of the same clone as previously stated was conjugated to Pacific Blue^{TM} dye eliminated signal from the sorted cells.

Following image acquisition at various parts of the functionalized areas of the coverslips, image was analyzed using ImageJ. Briefly, every cell (except morphologically apoptosis like cells displaying high number of granularity) in each snapshot were analyzed by drawing a circular ROI allowing to measure the intensity of the Cy5-dye fluorescence. An additional circular ROI of similar size to one of the cells was drawn on an open space of the same snapshot to obtain the background level intensity. Each circular ROI of the cells was normalized to the background of each image and the normalized intensity was obtained for each cell and the average was taken over all the snapshots of the particular condition. Cells displaying relatively increased normalized intensity (indicating separation of the quencher from the fluorophore) correlates with sufficient force (exceeding a threshold force) applied by the cell to unfold the hairpin and fluoresce (**Figure 14**). This depicts a molecular tension probe behaving as a switch

element reporting tension as a digital readout. The intensity from the reversible tension reporters is linearly proportional to the number of each receptor molecules exceeding a threshold force with the ligand on the surface depicted by each ligand linked probe engaging a single receptor. This is ideally suited for determining the force displayed by the cell mediated by the receptor/ligand interaction. The oligonucleotide's nucleobase sequence at the hairpin provides the freedom to tune the force-response function by varying the number of sequences.

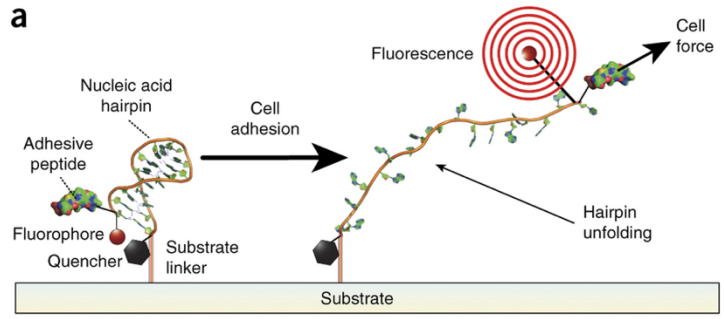

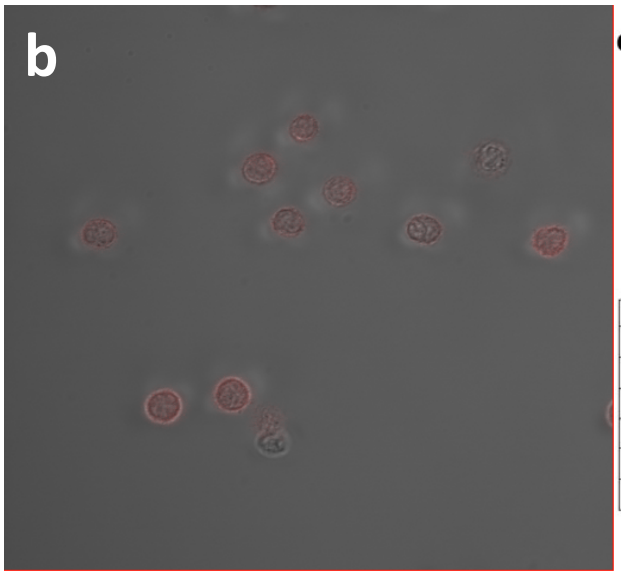

c

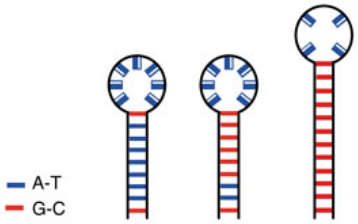

ID	22% GC	77% GC	100% GC
Length (mer)	25	25	28
ΔG (kJ mol^{-1})	21.9	49.6	95.2
Calc. $F_{1/2}$(pN)	4.2	9.6	16.0
Calib. $F_{1/2}$(pN)	4.7±1.7	------	13.1±2.1
$QE_{Cy3B\text{-}BHQ1}$%	95.3±0.1	95.2±0.1	97.1±0.5
$QE_{Cy5\text{-}QSY21}$%	94.1±0.2	95.3±0.3	94.8±0.3

Figure 14. DNA force probe. (a) Schematic depicting DNA-force probe linked to an adhesive peptide and following adhesion, the unraveling of the hairpin structure to allow fluorescence to take place. (b) Representative image of cells bound to DNA-force probe fluorescing. (c) Variation of the A-T and G-C content influences the degree of forces required to open the hairpin structure. (a) Adapted from [1]. (c) Adapted from [2].

3.2.9 *in-vitro* surface-bound pMHC T cell stimulation

The technique utilizes the interactions of selective proteins and as a result, cytokine production of T cells will be observed. The assays employs T cell function readily following the interaction with the ligand to observe detection of cytokine synthesis, in this particular case IFN-γ, by intracellular cytokine staining (ICS). This assay will be performed by well-plate assay, in which protein of interest are surface-bound coated. Using flat bottom well plates (48 or 96 tissue culture treated), biotin-BSA solution is initially covered by incubating the solution for 30 mins in incubator set at 37°C and with 5% CO_2. After washing the solution with PBS, streptavidin is then incubated similar to biotin-BSA. The last step involves incubating the biotinylated protein of interest either at the same time in the incubator or in 4°C overnight. After final washing with PBS, cells are added to the functionalized wells for 16-18hrs of stimulation. Followed by stimulation, cells are acquired for various staining including live/dead (L/D), surface protein markers and intracellular proteins, particularly ICS of IFN-γ. L/D staining was analyzed using the APC-Cy7 channel, antibodies against CD3 was

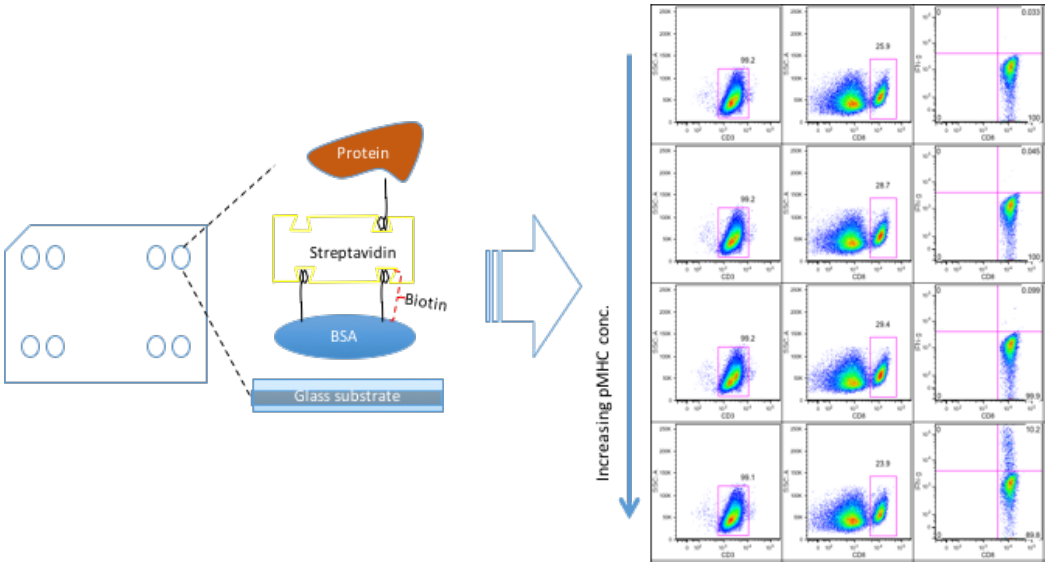

Figure 15. Schematic of reagent coating on well plate. A well plate zoomed into a particular schematic depiction of the protein coating with various reagents. Same coating reagents are used for microfluidic device. In the case of this study, the protein depicted on the image was substituted with biotinylated pMHC monomers.

fluorescein isothiocyanate (FITC) conjugated, for CD8 is peridinin chlorophyll protein complex (PerCP) -Cy5.5 conjugated and for IFN-γ is allophycocyanin (APC) conjugated. Using Aria (BD), flow cytometry of the multi-fluoresce stained samples are acquired and analyzed by FlowJo software (**Figure 15**).

3.3 Statistical analysis

Conducted statistical tests employed the use of Student's t-test or one-way ANOVA. Bootstrap was implemented to lifetime measurements of the force-clamp assays mostly due to limited number of observations and how we can estimate some quantity like the mean for the data set population from which the data was drawn. Thereby, by resampling with replacement from the data set, a population distribution can be simulated. We established 50 as the value of the number of bootstrap samples to be used in computation to obtain mean and the standard error of the mean. Box (3^{rd} and 1^{st} quartile for top and bottom with median in the middle) and whisker (maximum and minimum values for top and bottom) data was utilized for some of the data presentation.

CHAPTER 4

KINETIC CHARACTERIZATION OF PP65 EPITOPE SEQUENCE VARIANTS TO HUMAN CYTOMEGALOVIRUS IMMUNODOMINANT CD8+ T CELLS

4.1 Introduction

Persistent viral infection such as EBV or herpes simplex virus utilize latent strategy to evade immune mediated cytolytic response. These viruses are expressed in low or moderate levels when presented by APCs and thereby, result in the survival for long-term due to corresponding low levels of CTL activation. Such mechanism is clear for their survival. However, not all viruses can adopt this strategy and therefore, induce an immune response that evidently leads to its clearance. However, viruses like HIV-1 and HCV adopt a different strategy that leads to their survival and that is by evolution. By mutations, these viruses adopt "survival of the fittest" strategy leading to an exhaustive state of the immune system, where no longer an immune repertoire can be generated or exists that can clear the infection. These mutations are sometimes a single alteration of the peptide sequence that leads to the failure of the CTL to respond. Yet, despite continuous exposure of CTLs in the repertoire, an effective response is failed to take place to eradicate the virus. Our objective is to understand how mutations influences the interaction that leads to disruption of a cytolytic activity. For such understanding, especially involving human and pertinent viral infections, it is difficult answering questions with experiment or mathematics alone. Therefore, the current disciplinary work for this study addresses these problems in the

context of persistent viruses in human by utilizing CMV model and mutagenesis study to understand better of the interactions that leads to decreased viral immune response.

CMV adopts a strategy similar to EBV and it is characterized by low or intermittent levels of its own antigen expression resulting in low levels of CTL mediated activation. Therefore, CMV persists in the host and awaits an opportunity for the immune system to be compromised. CMV has evolved to take over the host immune system, remain latent and occasionally reactivate at which point 10% of the T cells population made up of CMV-specific T cells counter the antigen presentation. The most dominant CMV viral peptide expression is the NLVPMVATV (NLV), which is the pp65 tegument protein found inside the capsid of the virus and this specific sequence is associated with the allele HLA-A*02:01. Although error prone mutations do not occur frequently for CMV when compared to viruses such as HIV-1 and HCV, natural infrequent mutations have been reported (more specifically of the NLV peptide) and shown to impact cytolytic function of the CMV-specific T cells. In the case of HIV-1 and HCV, mutations lead to chronic development of the disease. Mutations of the viral peptides has been linked to impair CTL recognition and this is usually associated with amino acid substitutions that either leads to CTL mismatch with the peptide or alteration of the amino acid at anchoring residues to the MHC leads to the loss of peptide. As for the first case where a single amino acid substitution impacts CTL recognition and its function, how a single amino acid alteration influences TCR interaction is not fully understood. As such, the objective of this study is to understand how TCR interaction with WT and mutant peptides influence CTL function. Using biophysical assays, TCR-pMHC interaction can be characterized to better illustrate how the interaction influences CTL function. By using human PBMC known to be

positively identified with CMV infection and use NLV along with its variant peptides with mutations at known hotspots, a better understanding of CMV-specific T cell can become obsolete in its response and how viral mutation at key amino acids can potentially lead to viral escape and increase its viral fitness.

Previous studies focused on characterizing biophysical parameters between TCR-pMHC interaction of transgenic T cell system and have utilized this concept in the context of thymus T cell development understanding the role of peptides that are categorized either as positive and negative selecting ligands [65]. These studies have focused on linking kinetics parameters from 2D assays to predict the response of T cells and have highlighted the importance of how 2D kinetics fare better correlation with T cell response than 3D kinetics. The study has been extended to observe the role of force on TCR-pMHC bond interaction lifetime and how the bond profile regulates T cell function [66]. The importance from the previous studies has highlighted parameters that influence T cell response using transgenic mouse model system and therefore, it is one objective of this aim to extend the study to human viral infection using CMV system to better understand and stem the physiological relevance of the biophysical parameters.

In the CMV model, the goal is to understand how immunodominant CMV-specific T cells that are enriched for recognizing NLV peptide interacts with both the WT and the its viral variants. The interaction between TCR-pMHC, like other receptor-ligand interaction, are constantly experiencing forces both from the environment and from cellular components that make up the membrane (i.e. lipid rafts) along with intracellular components like cytoskeletal components. It has also been shown before that the synchronous harmony from both the critical force and sufficient lifetime are crucial to

calcium flux [66]. As such, for the CMV model, these parameters will be analyzed along with binding kinetics to better understand how these parameters correlates and influence the functional outcome. In this study, we hypothesis that mutations of the viral peptide not only influence 2D affinity, but under tension force of the TCR-pMHC interaction disrupt sustainability of the optimal critical force and lifetime to effectively induce a proper T cell response. To provide a better definition of optimal T cell response in the context of human viral infection using human PBMC samples, the following aims are tested: 1) 2D biophysical assays provide higher sensitivity than 3D methodologies; 2) Characterize 2D affinities for activated polyclonal NLV-specific T cells to WT and variants from different donors; 3) Characterize application of native force experienced by T cell when interacting with the pMHCs used in the previous aim; 4) Characterize under a range of force and map the profiles for the interaction stated in the previous aims; 5) Evaluate functional response of activated NLV-specific CD8+ T cell to each of the pMHCs stated in the previous aims. Comparison of sensitivity to the 2D assay used to 3D assay was done by using 2D micropipette assay to conventionally used 3D staining method to measure the frequency of antigen specific T cells, tetramer staining. Development of tetrameric pMHC complexes has provided a snapshot view of peptide-specific CTL distribution. However, similar to another 3D methodology (surface plasmon resonance), sensitivity is limited to this 3D approach for detection. Our 2D approach used in this study to obtain 2D kinetic parameters resulted in higher sensitivity, even reporting detection and affinity not originally seen with one of the variants (T8V) [49].

Obtaining 2D affinities was achieved utilizing 2D micropipette adhesion frequency assay using human PMBCs that were pulsed with NLV peptide to enrich NLV-specific T

cells, and RBCs with various concentrations were covalently coated with biotinylated pMHCs. The effective 2D affinity of NLV-enriched CTLs to both WT and variants were measured from 3 different donors. Due to polyclonal nature of the system varying from donor to donor, the 2D effective affinity was within the same magnitude of order of all 3 different donors.

Using DNA-force probe technology allowed us to characterize the natural generation of force the T cells applied to pMHCs bound to DNA-tension force probes, designed to fluoresce if set force tension threshold can be sustained for the receptor-ligand interaction. We observed that activated NLV-specific T cells sustained bond interaction and strengthened bond interaction for two of the three pMHCs focused on this study.

To characterize the force-lifetime profile under various clamped forces, BFP was utilized using the same CTLs as for the other assays, but the pMHC was covalently linked to streptavidin coated bead that was on a hypotonic induced RBC that was used as a force transducer with a known spring constant. All three peptides exhibited catch-slip bond profile and the lifetime at the critical force was measured for the three different donors.

To understand the functional output following interaction with each of the pMHCs, we were interested in understanding the IFN-γ cytokine release. This cytokine has been linked to be released following CTL activation to block viral replication. To characterize this output purely from TCR-pMHC interaction, we used biotinylated pMHCs that are plate-bound to initiate CTL activation and utilized ICS methods to obtain the frequency of cells exhibiting cytokine production.

Altogether, the approaches stated above provide a unique perspective and understanding of how viral variants utilize amino acid alteration to influence TCR recognition and influence functional outcome.

4.2 Results

4.2.1 2D biophysical assays provide improved sensitivity compared to 3D techniques

To initially measure the frequency of NLV-specific CTL, NLV pulsed PBMCs were stained for CD3, CD8, and the NLV tetramer. From the lymphoycte gating placed, CD3 staining was split it into low and high CD3 levels based on two distinct populations observed. By gating the CD8 population for both the high and low CD3 expressing populations, two different populations of NLV tetramer frequency was observed. For the $CD3^{high}/CD8^{high}$ population, not only a portion of NLV-specific CTLs were observed, there was almost >70% of the CD8 population that consisted of NLV-tetramer negative population. However, for the $CD3^{low}/CD8^{high}$ population, >70% of the CD8 population consisted of NLV-tetramer positive population. It has been reported that activated CTLs downregulate CD3 expression [67] and that could be associated with the observation that higher frequency of NLV-specific CTLs were seen from the $CD3^{low}/CD8^{high}$ population when the PBMCs were pulsed with NLV peptide. Since frequency of NLV-specific T cells was detected higher of the $CD3^{low}/CD8^{high}$ population, frequency of cross-reactive or pMHC-specific tetramers were stained for the other viral variants were measured albeit at higher concentration for some due to affinity of the peptides (T8V, M5I, and P4FT8V).

As for determining the sensitivity from the 2D micropipette adhesion frequency assay, we obtained the result from 40-100 CTLs that generated binding frequency greater than the background level. The background level of binding frequency was determined by using either streptavidin-alone coated RBCs or RBCs coated with a self A2 peptide. Binding adhesion was determined during the retraction phase of the RBC following

RBC/T cell contact and if the RBC adhered seen formation of tether when RBC was pulled back. Binding frequency was measured after 30 cycles of the following sequences that involved contact, impingement, and retraction. CTLs were sorted using tetramer stained sample as the template to sort either $CD3^{low}/CD8^{high}$ or $CD3^{high}/CD8^{high}$ population and the frequency of this assay was compared to that of tetramer stained sample. For $CD3^{high}/CD8^{high}$ population, 2D assay displayed higher sensitivity than 3D tetramer (~3-fold increase). As for the $CD3^{low}/CD8^{high}$ population, we observed similar sensitivity between the two assays for CTLs recognize NLV-MHC (**Figure 16**). Taken together these two findings illustrate that activated CTLs recognizing pulsed peptide in the form of MHC complex are similar, however, in the context of $CD3^{high}/CD8^{high}$, where

mixture of NLV specific and non-cognate specific T cells are mixed, the 2D assay prove to more sensitive than 3D detection.

For the variants, only $CD3^{low}/CD8^{high}$ population was analyzed for comparison. This is due to the technical limitation output if $CD3^{high}/CD8^{high}$ population were sorted for 2D micropipette adhesion frequency assay as this sorted sample will have decreased proportions of selecting NLV-specific T cells to measure 2D affinity. Especially when measuring 2D affinities for variants that have very low binding propensity for majority of the polyclonal subset. When comparing the sensitivity of the $CD3^{low}/CD8^{high}$ population from the two different assay across the viral variants, we observed that 2D assay has shown better sensitivity than the 3D counterpart.

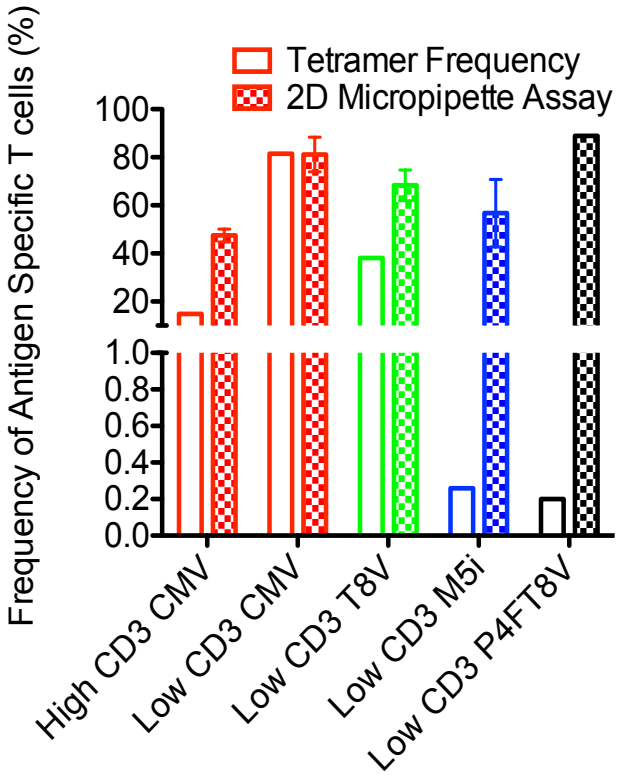

Figure 16. Comparison of antigen specific T cell frequency from Tetramer staining and 2D Micropipette assay. Comparison of high and low CD3 population of NLV staining to 2D micropipette assay. Additionally, tetramer staining comparison to 2D assay for the different altered peptide ligands for $CD3^{low}/CD8^{high}$ cells.

Overall, NLV-pulsed polyclonal T cells stained with tetramers of NLV and variant peptides to estimate the frequency of reactivity to the NLV and cross-reactivity to the variant peptides. As expected, NLV tetramer had the highest frequency compared to that of the mutants. Of the viral variants, T8V tetramer showed higher frequency of cross reactivity than M5I and P4FT8V.

4.2.2 Disruption of molecular bonds impairs 2D effective binding affinity

In order to quantify the bimolecular interaction exhibited between the enriched CMV-specific T cells to that of the different pMHCs, we used 2D micropipette adhesion frequency assay (**Figure 17**). For the majority of the analysis, $CD3^{low}/CD8^{high}$ population was analyzed due to enriched NLV-specific T cell observed from tetramer staining. Similar to the results of tetramer staining, 2D effective affinity of NLV peptide binding to CMV-specific T cells exhibited a log order higher than T8V peptide and two-log order higher than M5I and P4FT8V peptide. Both tetramer staining and 2D measurements indicate that mutations at the hydrophobic amino acid residue that directly contacts with the TCR has more profound impact on CMV-specific TCR recognition, more so than mutations at residue 8, where alteration of valine at this position to isoleucine resulted in disruption of hydrogen bond networks [49]. It is also observed that mutation at the 4^{th} residue, another known hotspot [49] known for forming hydrogen bonds to a lesser extent than that of residue 8, from proline to phenylalanine of the T8V variant resulted in lowering the 2D affinity to the level of M5I variant. This double mutant was predicted by Paul Cardenas-Lizana in the purpose to identify the impact and the extent of the role the 4^{th} amino acid hydrogen bond contributes with the TCR affinity and later bond formation [49]. Clearly, the replacement to a bulky residue resulted disrupting its hydrogen bond, in addition to the hydrogen bond disruption at residue 8, resulted in lower affinity when compared to that of its single mutation counterpart.

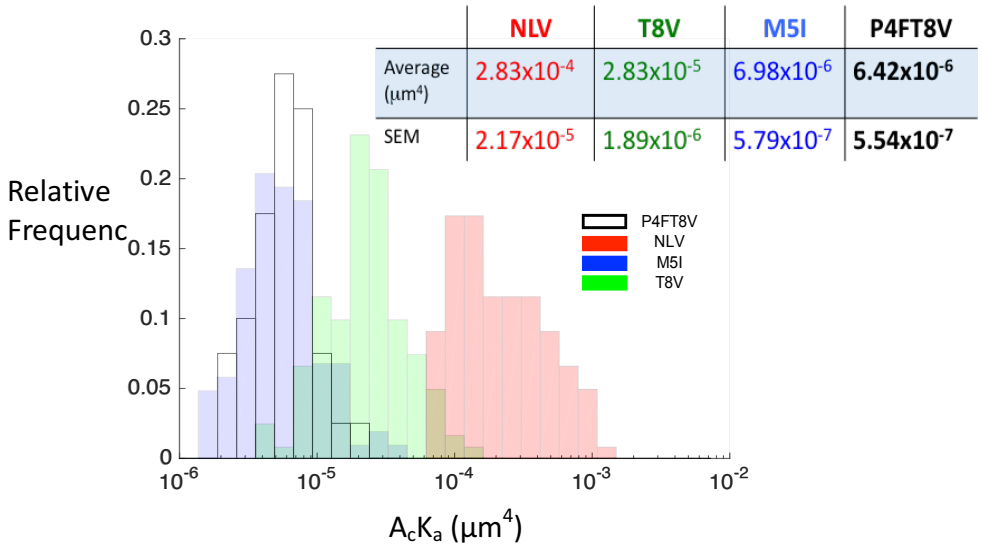

Figure 17. Histogram of 2D effective affinity of pMHC to NLV-pulsed CD8+ T cells of Donor 9. Polyclonal NLV enriched, $CD3^{low}/CD8^{high}$ sorted cells were measured for 2D effective binding affinity for the WT and mutant peptides. Table inset provides quantitative values of each peptide to the enriched polyclonal cells.

The results shown in figure 17 shows the result of the 2D effective affinity from one individual donor (donor 9) and therefore, the measurement obtained most likely does not reflect as a universal number for all populations. Due to the possibility of donor to donor variations, we gathered two additional donors that are known to be CMV positive and set out to analyze their respective 2D effective affinity. What we observed from $CD3^{low}/CD8^{high}$ populations of other two donors (donor 209 and donor 42) was that their 2D affinity was statistically different from donor 9. However, all three donors had the same log order magnitude and the variation from different donors might rise from different clones with varied proportions, in which certain subsets of clone may exist in different frequencies between donors (**Figure 18**).

Additionally, we observed the two levels of CD3 population for analysis to determine if activated CTLs had differing 2D effective binding affinity than CTLs with higher expression of CD3. For the $CD3^{low}/CD8^{high}$ population or the activated group, 2D effective binding affinity was $2.93x10^{-4}$ and in comparison to the $CD3^{high}/CD8^{high}$ population, 2D effective binding affinity was $2.73x10^{-4}$ (**Figure 19**). This indicates that

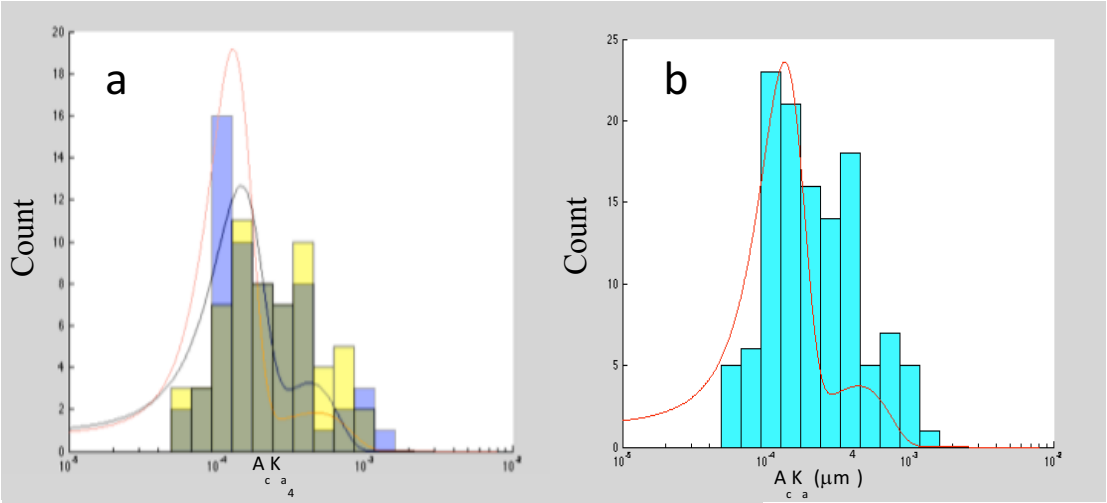

Figure 19. Binding affinity histogram of both CD3^{Low} and CD3^{High} populations. (a) Overlay of the range of affinities measured from CD3^{low} (yellow bars) and CD3^{high} (blue bars) population. (b) The cumulative data of the two populations.

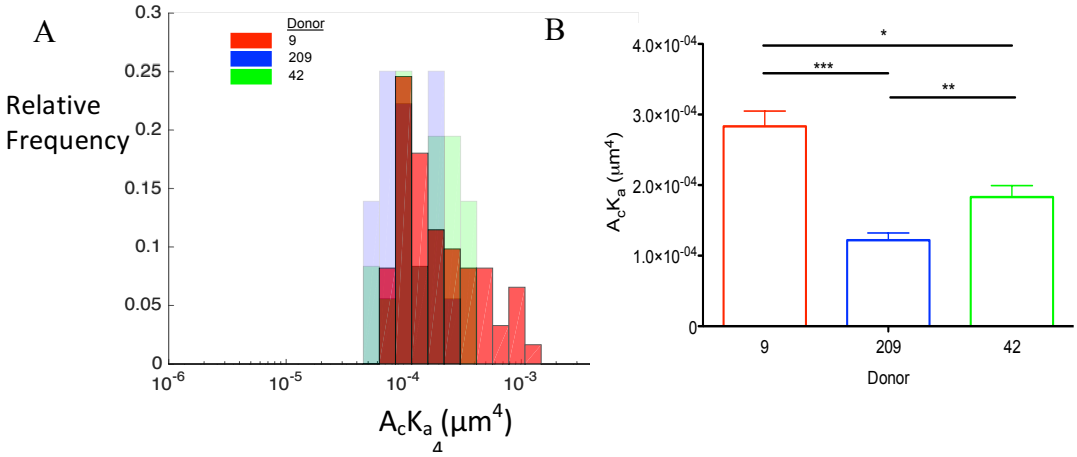

Figure 18. Measurement of 2D effective affinity of different donors. (A) Histogram of polyclonal enriched CD3^{low}/CD8^{high} binding to NLV-MHC. (B) Bar graph depicting the average 2D effective binding affinity among the three donors. Error bars represent the SEM.

even after activation, the 2D effective binding affinity does not vary. However, there is always possibility using a higher coating of the NLV peptide could capture lower affinity TCR clones in the CD3^{high}/CD8^{high} population.

4.2.3 Viral variants influence and disrupt bond lifetime interaction of NLV enriched CTLs

In order to understand how different hotspots of the peptide sequence influence bond lifetime under cell's own endogenous force, sorted $CD3^{low}/CD8^{high}$ cells were subjected to interact with the pMHC bound to DNA force probe designed to rupture at pulling force of 16pN. We chose 16pN DNA force probe to understand if tension can be prolonged to reach this level as we have previously reported from our OT-1 system to have reached this level force threshold to fluoresce and in another study, similar force level induced calcium flux [66]. Sorted cells were allowed to interact with pMHCs and if sufficient tension force threshold is met, the hairpin loop opens providing increased signal intensity indicating sustained increase in lifetime stemming from this interaction that reaches or exceeds the set threshold. Such was the case for the sorted cells interaction with NLV and M5I indicating TCR interaction with these peptides display prolonged increase in bond lifetime until reaching 16pN. However, sorted cells exhibited decreased intensity with T8V indicating that the bond lifetime between the interaction does not reach prolonged lifetime reaching towards 16pN (**Figure 20**). However, results from DNA force probe assay for both NLV and M5I indicates that the lifetime is prolonged towards reaching the critical force.

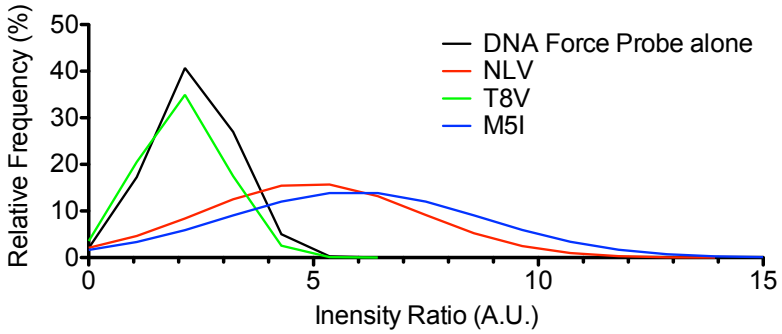

Figure 20. Histogram of DNA fluorescence probe intensity for varying pMHCs interaction with $CD3^{low}/CD8^{high}$ population. Fluorescence intensity histogram of enriched polyclonal population of NLV pulsed PBMCs.

4.2.4 Characterizing bond lifetime under range of forces of various viral pMHCs of its interaction with NLV enriched CTLs

To fully elucidate the force-lifetime profile stemming from the DNA force probe assay results, we used biomembrane force probe to characterize over a long range of force lifetime profile. Initially we wanted to characterize at the critical force (set at 15 pN) to understand the lifetime of the different pMHCs and from different donors. Comparing donor 9 with the other donors (donor 42 and 209), we observed that the lifetime of the WT pMHC to the sorted $CD3^{low}/CD8^{high}$ samples was overall comparable, with the exception of donor 42, which statistically significant (**Figure 21**). As for the sorted sample binding to M5I-MHC, we did not observe any significant differences among the donors. However, interaction with T8V-MHC showed significance over the three donors. Altogether, the results indicate that the different donors have varied frequencies of clones that result in the varied lifetimes observed, this notion is emphasized especially with interaction with T8V-MHC. Additionally, we observed that the alteration at the 8^{th} residue, where the dense hydrogen bond network is disrupted, collectively among the three donors depicts lifetime is not sustained for long duration as compared to the interaction with M5I-MHC, where the hydrophobic interaction is

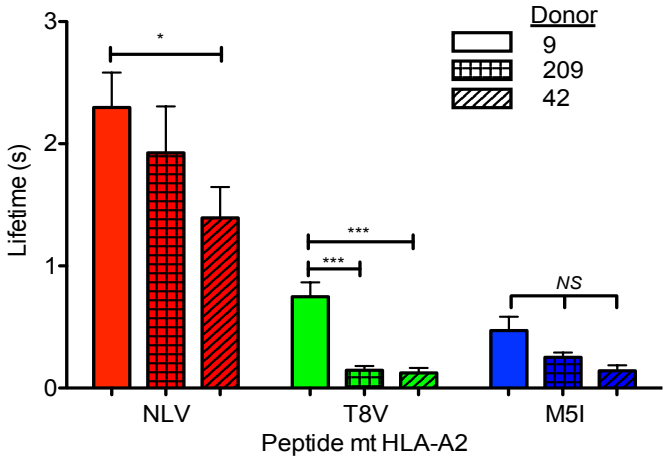

Figure 21. Comparison of critical force bond lifetime of different donors of different peptides. Clamp force at 15pN to characterize bond lifetime of different donors to the WT and the single mutant.

disrupted. This is surprising when comparing these results to that of the 2D affinity, where T8V group showed a log order higher than that of the M5I.

As such, we next characterized the lifetime profile over range of forces to categorize the bond profile and we selected donor 9 samples to characterize due to its abundance of NLV-specific T cell frequency from tetramer staining. TCR binding to NLV-MHC displayed catch-slip profile, with critical force situated at 15pN with lifetime 2.6 sec. In the case for M5I interaction with the CMV-specific T cells, we observed lifetime being prolonged at similar critical force (**Figure 22**). However, the lifetime duration is significantly lowered for this particular interaction at the critical force resulting from the disruption of the hydrophobic interaction. This once again, implies, the hydrophobic interaction from methionine contributes in strengthening the bond and potentially plays an essential role in propagating signal transduction.

The effect of disrupting the hydrogen bond network resulted in the critical force reaching well below the threshold for M5I and NLV (**Figure 22**). Based on this effect on lifetime following mutation at the 8th residue to valine, which is a smaller amino acid in

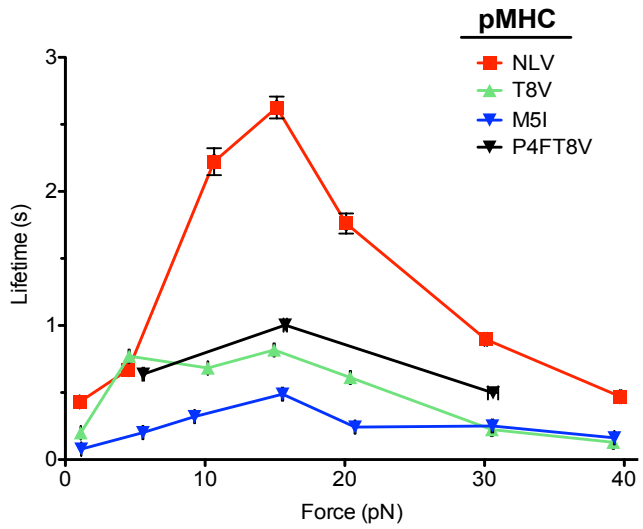

Figure 22. Bond mechanics profile of donor 9 samples to the various peptides. Sorted polyclonal NLV-specific T cells interaction with the various peptides under different force clamps was characterized.

length than threonine, we can potentially link this result of the effect of threonine on forming new hydrogen bonds as the force is increased.

Lastly, we measured an additional alteration of an amino acid to a previously mutated peptide (T8V), the resulting double mutation, P4FT8V. The hypothesis, based on molecular dynamic simulation performed by Paul Cardenas-Lizana, was to understand if this particular mutation can help shift the critical force to the level of NLV- and M5I-MHC. By mutation to phenylalanine from proline, the hypothesis is to further enhance the effect of hydrogen bond formation of proline by introducing a longer amino acid, such as phenylalanine. This result of the double mutation impacted the critical force to be shifted to the level of both NLV and M5I. However, due to disruption of the hydrogen bond network at residue 8, no additional hydrogen bonds are formed preventing increase in lifetime to the level of the NLV-MHC.

In summary, key hotspots in the peptide sequence contribute both in stability and prolonging lifetime under force. Both are critical components in influencing signal propagation through the TCR for the CTL to effectively induce cytolytic response to the viral infection.

4.2.5 Cytokine production response to interaction with various viral pMHCs

Many system shows that stimulation with tetramer alone does not stimulate cytokine release, although the addition of exogenous peptide and co-stimulation produces a strong response. Here we show that surface bound pMHC can stimulate NLV specific T cell to generate cytokine secretion. In order to understand the functional response stemming from CMV-specific T cells interaction with NLV and the mutant variant pMHCs, we evaluated the production frequency of IFN-γ of CMV-specific T cells via ICS (**Figure 23**). ICS was conducted following incubation of the entire pulsed PBMCs on plate wells coated with respective pMHCs at various concentrations. After overnight stimulation, CMV-specific T cells incubated with NLV-MHC had the highest production of IFN-γ at very low

concentrations (especially 0.01 μg/ml) in comparison to the other variants. Mutant variant T8V displayed the second highest production of IFN-γ, albeit at very high concentrations to get similar IFN-γ frequency as the NLV-MHC (10 μg/ml of T8V-MHC vs. 0.1 μg/ml) By comparison, mutant variant M5I had the least production of IFN-γ among the different pMHCs. To obtain similar frequency of cells generating IFN-γ as the NLV-MHC, 10 μg/ml of the variant is used to get approximately 10% frequency, which was achieved using the NLV-MHC at a concentration of 0.01 μg/ml. Altogether, these results indicate that the hydrophobic residue methionine plays a central role in recognition and function and its disruption significantly influence an effective response.

4.3 Discussion

The immune system of a host initiates a massive polyclonal T cell response following viral infection, however the specificities of only a small percentage of these activated cells are known in various diseases and they are usually the immunodominant subtypes. In the case of CMV infection for humans with HLA-A*02:01, immunodominant restricted epitope derived from CMV protein is NLV specificity during steady state and

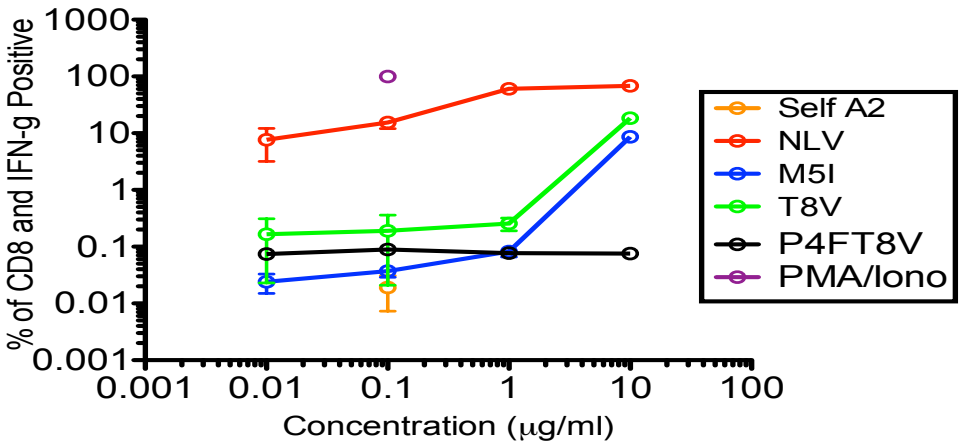

Figure 23. Intracellular cytokine staining of antigen specific T cell from surface coated pMHC stimulation. Percent of $CD8^+$ T cells that secretes IFN-γ from entire CD3 and CD8 population. Positive control used here is PMA/Ionomycin and the negative control is an irrelevant pMHC sharing similar allel as the cognate pMHC.

pathological situations associated with CMV reactivation [68]. A large fraction of NLV-specific T cells derived from numerous individuals expressed a "public" TCR feature that exhibited full conservation of the TCRα chain junctional region, however, TCRβ chain junctional region varied and highly diverse. At low detection limit, 2D micropipette has a higher sensitivity detecting antigen specific T cells than tetramer staining. Upon reactivation of CMV-specific T cells, a clonal focusing takes place where public TCR clonotypes exhibiting high affinity for the antigen dominates, implying that TCR affinity plays a central role in repertoire focusing. To mimic this phenomenon, *in vitro* stimulation with NLV peptide increase the frequency of dominant private NLV specific T cells from various CMV-positive donors to understand the kinetic interactions of these polyclonal T cells to WT peptide and epitope variants. This provides a true understanding of how varied the 2D effective affinity from a given individual highlighting the variation and the average parameter from a donor.

Unlike HCV, CMV infection typically do not constitute mutations stemming from HCV inherent RNA-dependent RNA error-prone polymerase. Therefore, CMV mutations, if occurring, is exerted by selection pressure from the environment or by drug selection. Immune response mediated selection pressure has been a mechanism to cause sequence variability and immune escape for both viral infection, tumor and autoimmunity [50]. To understand the principles of a polyclonal T cell response interaction with WT and its variants, this study focuses on an infrequent naturally occurring mutation of the NLV peptide and a synthetic mutation to understand how amino acid substitutions at non-anchoring residues influences biophysical and functional analyses.

The tetrameric assay has influenced our knowledge of human disease and has provided insights into the frequency, phenotype, and functions of $CD8^+$ T cells, especially in the case of viral infections. Alongside, 3D assays like biacore, has provided kinetic parameter using purified TCRs. Both these assays lack sensitivity and particularly biacore experiments can utilize a single TCR at a time. Due to clonal diversity of T cells found

within a host, it is imperative to address the kinetics on average and additionally, characterize the effective cross-reactivity with altered-peptide ligands.

To understand how T cell viral reactivity relates to 2D binding parameters and to directly compare them, kinetic analyses was performed of a panel of viral antigens to a polyclonal enriched NLV-specific T cells. Panel of viral epitopes utilizes the WT and its variants. Mutation at the 5^{th} residue from methionine to isoleucine has previously shown to result in a decreased lytic function [50]. Methionine plays an important role in forming a hydrophobic interaction with the immunodominant public NLV-specific T cells and it has been identified as a hotspot in the amino acid sequence of the NLV epitope [49]. Mutation at this residue provides insight that methionine plays a central role in establishing a stable bond between the TCR and the pMHC. Additional hotspots in the NLV peptide sequence are at the 4^{th} and 8^{th} residue, however, of the two, threonine at the 8^{th} residue forms a network of hydrogen bonds with the TCR and thus, we predicted that this residue plays a central role in formation of new bonds that strengthen the lifetime as force increases between the TCR and pMHC [49]. Our results show us that, by mutation of this residue from threonine to valine, we observed the catch bond formation was capped off before reaching the critical force observed with the WT peptide interaction.

The effective 2D affinity correlates positively with the functional response. By focusing on the lifetime measurement at the critical force (15 pN) of donor 9, the functional response correlates with the duration of the lifetime, as well. This might imply that although affinity is an important component of signaling that has been well characterized to correlate with function, the force induced bond-lifetime results indicate that increased lifetime at critical force also correlates with increased functionality. However, when considering all the parameters, 2D effective binding affinity threshold has to be met followed by the duration of the lifetime to induce the proper cytokine function as suggested by the data.

Application of force provides more insight on the TCR/pMHC interaction providing potential mechanisms viral mutations could influence binding kinetics and how that translates to impacting functional response of the CTL. Mutations at hotspots that contributes heavily in bond formations impacts the profile differently depending on the peptide and its alteration. Ultimately, viral mutations take place to evade immune response and help facilitate the survival of the virus. Current conventional methodologies (3D assays) provide basic kinetic parameters to understand the propensity of the binding. By utilizing 2D assays, especially understanding how force-clamping impacts bond survival paints a unique perspective of how mutations disrupts the initial recognition.

CHAPTER 5

2D ANALYSIS OF TCR-PMHC INTERACTION REVEAL DIFFERENTIAL CELL FATE GOVERNED BY COMPARTMENTALIZATION

5.1 Introduction

After viral clearance, an essential component of the immune response, contraction of the host's adaptive immune cells takes place setting up a repertoire moving forward to combat upcoming secondary infection. However, during and following viral clearance, the environment is modified in which the cells reside and cells from different environment can influence their behavior and function. However, how this occurs and what triggers their modulation has not been fully elucidated. To understand how viral infection influences shaping the immune cells, LCMV mouse model infection is utilized, as well as, adoptive transfer method of viral-specific monoclonal transgenic cells to track and conduct ex-vivo studies. Primary focus on T cell are from those residing in spleen, as it mostly known here to play a prominent role in facilitating induction of an adaptive immune response. Close inspection of the anatomy of the spleen shows two distinct structures: WP and RP. Blood enters the spleen through the marginal sinus and travels through the RP away from the WP to return back to the vasculature network via venous sinuses. At the border of marginal sinus and WP, APCs capture pathogens and within the WP, initiate productive contact with their cognate lymphocytes and provide signals within this niches to initiate differentiation to CTLs [44].

As spleen contains two functionally and morphologically distinct compartments, the goal of this study is to understand the kinetics of viral-specific T cells, specifically adoptively transferred P14 cells that is cognate T cell recognizing LCMV infection, from these compartments over the course of the infection. Additionally, correlate the functional effect of cells residing in their respective compartments. In the process of this immune response, an additional goal is to elucidate the mechanism that contributes to the effect observed.

5.2 Results

5.2.1 Localization within anatomical compartmentalization of $CD8^+$ T cells exhibit differential TCR-pMHC interaction during early immune contraction phase

To understand the kinetics of CD8+ T cell undergoing the influence of viral immune response, naïve mouse was adoptively transferred with P14 cells and infected with LCMV Armstrong infection to induce an acute viral immune response. Following days after infection, adoptively transferred P14 cells were sorted out from their respective compartment (i.e., WP or RP) and were subjected to measuring 2D binding affinity. Adoptively transferred P14 cells to host without infection was also conducted to observe how naïve P14 cells 2D kinetics fared from respective compartments. To determine the 2D affinity of the P14 TCR from each respective compartment, RBCs coated with biotinylated gp_{33-43} (gp33) was utilized as a surrogate APC. The H2-D^b MHC was mutated in most cases to focus on the bimolecular interaction between TCR and pMHC. The 2D effective affinity was measured from each compartment during the three main phases of the immune response: naïve, effector, contraction and memory phase of the T cell differentiation.

Monoclonal P14 T cells exhibited modulation in 2D TCR affinity over the course of the immune response both in the WP and RP. More evidently, 2D TCR affinity of RP P14 T cells during early contraction phase (9 and 11 dpi) exhibited markedly higher than

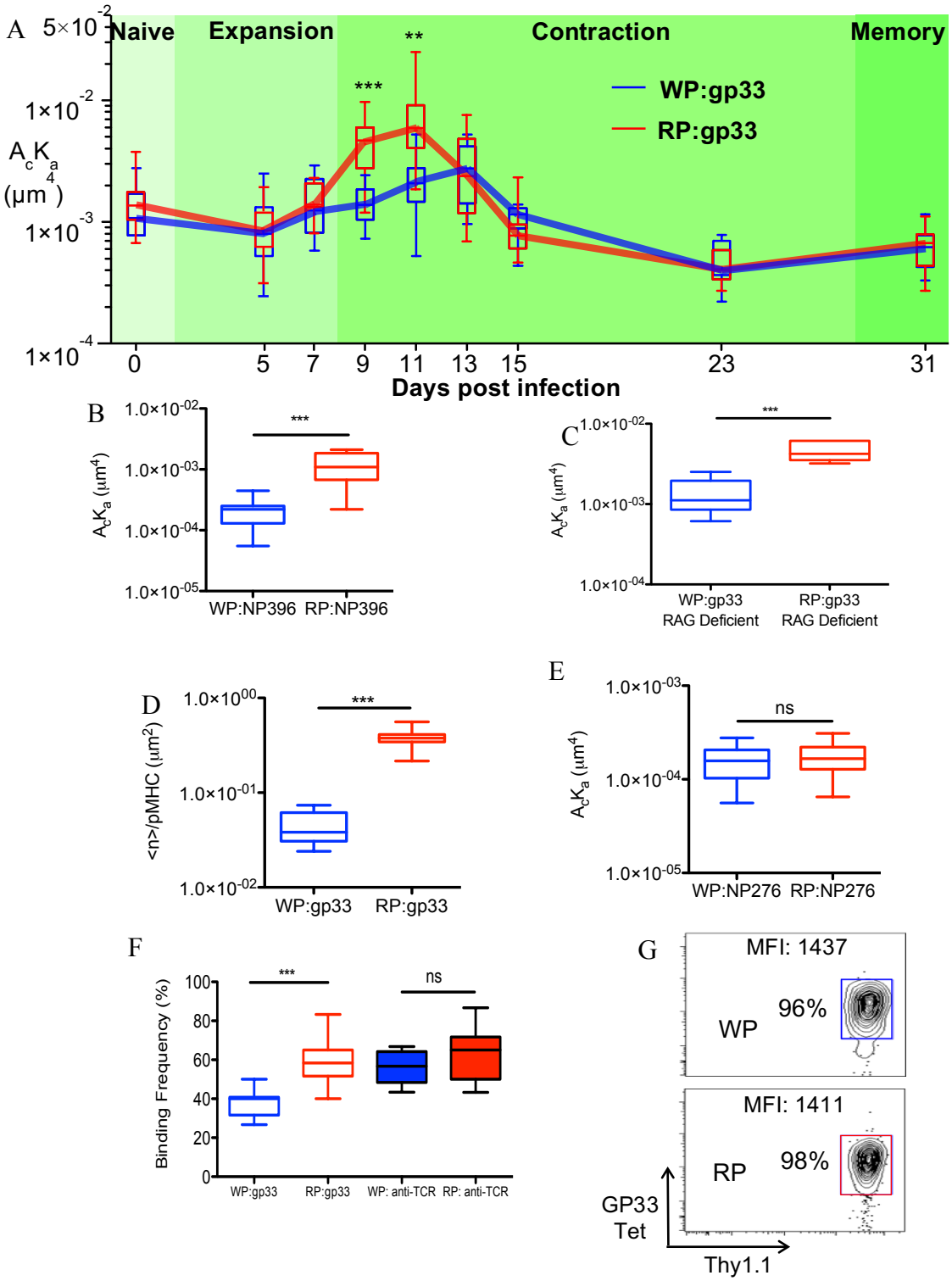

P14 T cells from WP (**Figure 24A)**. Furthermore, use of gp33-tetramer staining resulted indistinguishable between the two compartments, consistent with the previous aim and reports that 2D mechanical-based assays provide more sensitivity than 3D assays to

Figure 24. TCR–pMHC interaction of LCMV specific T cells from the WP (blue) or RP (red) measured at the indicated dpi. (A) The red line depicts the 2D effective binding affinity of adoptively transferred P14 cells sorted from the RP, whereas the blue line depicts P14 cells from WP. Cells binding to gp33-MHC utilizes a mutated MHC preventing binding between CD8 and MHC. (B) Endogenous NP_{396}-specific T cells sorted from their respective compartments were measured of their 2D effective binding affinity at 11dpi; the mouse was also adoptively transferred of P14 cells. (C) P14 T cells that are of RAG-1-deficient were adoptively transferred and following 11dpi, transferred cells from their respective compartments was analyzed for their $A_c k_a$. (D) Average number of bonds normalized to the pMHC density comparison of P14 T cells to gp33 pMHC, trimolecular interaction involving TCR-CD8-pMHC. (E) Adoptively transferred P14 T cells binding to non-cognate peptide MHC to evaluate the binding between CD8 and MHC H2-D^b allele at 11dpi. (F) Comparison of P14 T cells binding to gp33 mutant MHC from respective compartments to that of P14 T cells binding to anti-TCR antibody. (G) Comparison of sorted P14 from respective compartments by tetramer staining.

discriminate TCR-pMHC interaction (**Figure 24G)** [69, 70]. Keeping the comparison between the two compartments, P14 T cells from WP and RP exhibited comparable 2D effective binding affinity during day 0 (naïve), 7 (effector), and 31 (memory) post infection along with other additional days (**Figure 24A**).

Additionally, following adoptive transfer of P14 cells and infection, endogenous LCMV specific T cells recognizing a different epitope from gp33 was also assessed at 11 dpi. By coating RBCs with $NP_{396\text{-}404}$-MHC, cells sorted from RP and WP were measured for their respective 2D effective affinity, which in result displayed RP cells exhibiting higher 2D effective affinity than WP (**Figure 24B**). The possibility of a second TCRα chain in TCR-pMHC interaction could potentially be one reason of the enhanced 2D affinity observed in RP. To test this notion, recombination activation gene (RAG)-1-deficient P14 was adoptively transferred and after 11dpi, 2D effective affinity was assessed from their respective compartments. The results of adoptively transferred RAG-1-deficient P14 cells also exhibited similar differences in 2D effective affinity from respective compartments similar to that of the wild-type P14 cells (**Figure 24C**).

In most experiments for the LCMV study, peptide is complexed with a mutated MHC, thereby eliminating the interaction between MHC and CD8. However, when measured using gp33 complexed with wild-type MHC against P14 T cells, involving tri-molecular TCR-CD8-pMHC interaction to take place, the average number of bonds normalized to the pMHC density differed as well between the two compartments (>7 fold shown in **Figure 24D**). Therefore, to investigate whether CD8 interaction alone with MHC exhibited similar observation, P14 cells were subjected to interact with $NP_{276-286}$ complexed with wild-type MHC capable of forming CD8 interaction, but not with the P14 TCR. This resulted in the differences being abolished between the two compartments

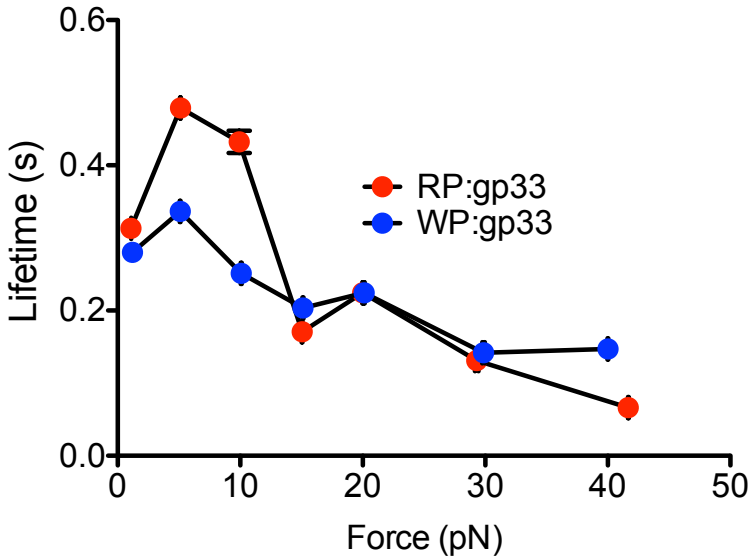

Figure 25. Force-clamp lifetime measurement of compartmentalized P14 cells following 11dpi. P14 cells sorted based on localization in RP or WP were characterized for their lifetime. Bootstrap implementation of lifetime measured at each force clamp.

indicating the differences observed were TCR-pMHC mediated (**Figure 24E**). To understand if TCR binding to other proteins, such as anti-TCR antibody, exhibited such differences, RBCs were coated with anti-TCR antibody. The result of this interaction also abolished the differences observed between TCR-pMHC from respective compartments (**Figure 24F**).

Being that gp33-MHC is a agonistic peptide for P14 T cells, the interaction between the receptor-ligand was evaluated for its bond mechanics under force and how the interaction is regulated due to the compartments they reside (**Figure 25**). Following 11dpi, sorted P14 cells from their respective compartments exhibited catch-slip behavior. Interestingly, cells from both compartments exhibited a catch behavior at an early force. The differences, however, was clearly seen when addressing the lifetime duration parameter. RP P14 cells exhibit longer bond lifetime than that of the WP P14 cells.

5.2.2 Local vs. systemic environmental effect on the enhancement of the 2D effective affinity of $CD8^+$ T cells to recognize potentially minute levels of antigens and viral escape variant

The RP compartment consists of blood-filled sinuses and play a distinct role in filtering RBCs. Additionally, being that the RP of the spleen is connected to the vasculature network of the host transporting cells from one organ to other sites, we also investigated the 2D effective affinity of antigen-specific cells found in peripheral blood to compare the kinetics observed within the two compartments of the spleen. At the height of the immune response (7dpi) and at 15dpi, P14 cells from peripheral blood exhibited similar 2D effective binding affinity as those of the cells from the respective spleen compartments. However, at 11dpi, P14 cells from peripheral blood exhibited the high 2D effective affinity just as P14 cells as the cells from RP, potentially depicting the notion that the increased enhanced recognition by P14 cells in circulation might be associated with targeting minute residual antigen presentation of the viremia (**Figure 26a**). The survival of viruses is dependent on the effectiveness of the immune recognition and if effective, viruses could be forced to mutate to evade immune response. If such scenario were to take place, the enhanced 2D effective affinity during early contraction from RP could facilitate recognizing escape viral variants with heightened sensitivity. To test this notion, a mutant of gp33 was used to observe how the viral variant impacts P14 cell recognition from each respective

compartment derived from the spleen. One previously observed natural viral variant of gp33 is gp35A (V35A), where at the 35th residue valine was substituted with alanine [47, 71]. Although P14 cells from both RP and WP exhibited lower 2D effective affinity for V35A when compared to that of gp33 following 11dpi, the differences between the RP and WP still held true, as RP displayed higher 2D effective affinity than WP when recognizing the viral variant V35A (**Figure 26b**).

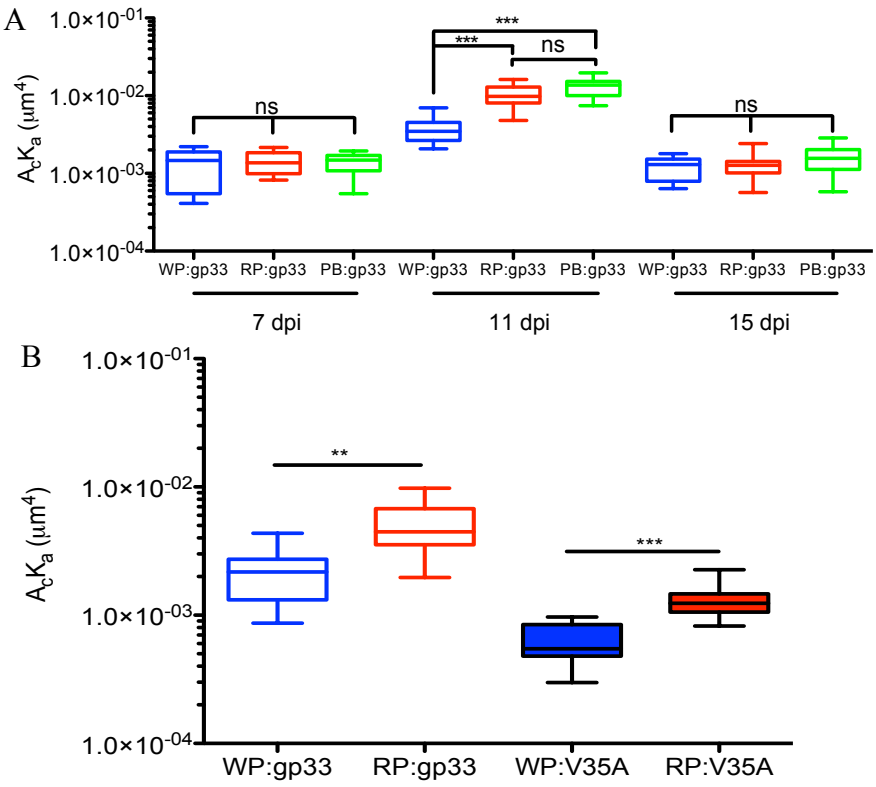

Figure 26. Kinetics of P14 T cells outside the local environment and recognition to mutation. (A) Adoptively transferred P14 T cells from peripheral blood exhibit similar kinetics to RP T cells and not WP from their respective days. (B) Adoptively transferred P14 T cells recognition to mutant peptide exhibit higher 2D effective binding affinity of populations from RP than WP following 11dpi.

5.2.3 Functional response of compartmentalized P14 T cells following recognition of cognate pMHC

As for the functional relevance of P14 T cells stemming from different compartments, following 11dpi, RP P14 cells exhibited increased calcium flux when compared to that of cells from WP (**Figure 27 a and b**). This supports the idea that P14 cells from RP are capable of efficiently targeting cells and signaling for lysis than cells from WP. Furthermore, RP P14 cells have higher proliferative capability following interaction with gp33-MHC than P14 cells from WP following 11dpi utilizing plate-bound pMHC stimulation (**Figure 28c**). Altogether bringing 2D effective affinity data and functional outcome following 11dpi, P14 T cells from RP exhibited higher 2D effective affinity than WP P14 T cells. This correlates with increased calcium signaling potentially for killing and proliferative capability.

5.2.4 Anatomical compartment effect on WP $CD8^+$ T cells by cellular and protein regulators

As the spleen is composed of different cells particularly residing in certain compartments, these cells that make up the compartments could potentially influence antigen-specific T cells to be mediated by direct contact or through cytokine release in the local microenvironment. The RP and WP are not only functionally and structurally distinctive, but as well as the cellular composition that make of it. Close inspection of the WP reveals an abundant level of $CD4^+$ T cells, which facilitate the priming of $CD8\alpha^+$ DC and in result priming of $CD8^+$ T cell activation. In comparison, DC also make up the composition of RP, however, circulating CD8+ T cells are found in higher frequency following the induction of the immune response and are frequently gaining access to secondary lymphoid organs in search for cognate antigens [45, 72]. Due to the presence of $CD4^+$ T cells in the WP having more pronounced contact with the $CD8^+$ T cells, ablation of $CD4^+$ T cell took place to observe the effect on kinetics of the adoptively transferred T

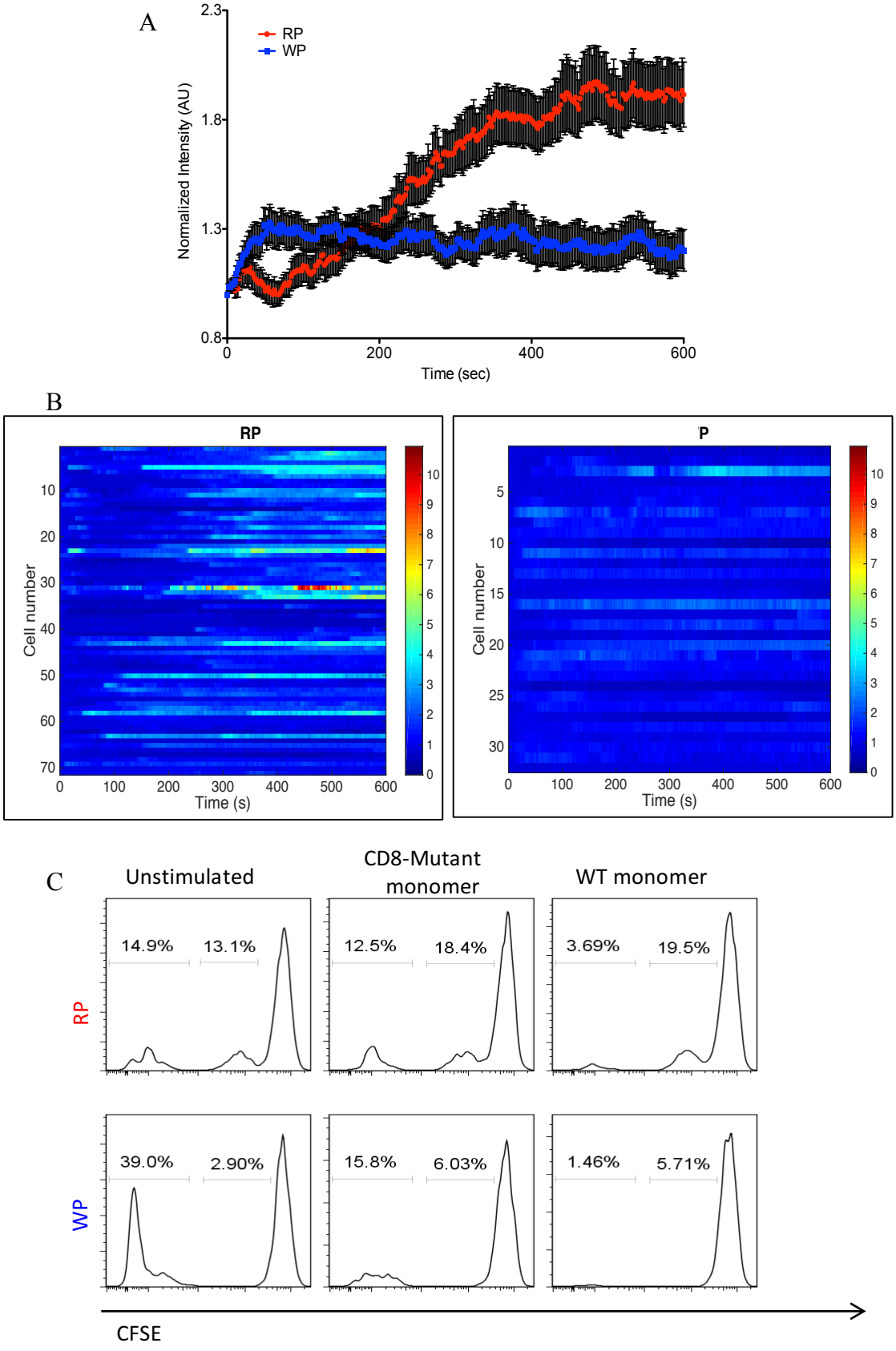
A
RP
WP
Normalized Intensity (AU)
2.3
1.8
1.3
0.8
0
200
400
600
Time (sec)
B
RP
P
Cell number
Time (s)
C
Unstimulated
CD8-Mutant monomer
WT monomer
14.9%
13.1%
12.5%
18.4%
3.69%
19.5%
39.0%
2.90%
15.8%
6.03%
1.46%
5.71%
RP
WP
CFSE

Figure 27. Compartmentalized P14 T cells response to antigen recognition. (A) The average fluorescence intensity of the cells analyzed in (B). Cells loaded with Fluo3-AM cytoplasmic calcium indicator. (B) Heat map for individual P14 cell response from respective compartments to peptide recognition over a course of the time period. Colors indicate low (blue) to high (red) cytoplasmic calcium indicators. (C) Respective compartments of adoptively transferred P14 T cells following 11dpi were incubated with CFSE dye and placed in wells coated with gp33-MHC and observed using flow cytometry following 3-day incubation.

cells following 11dpi (**Figure 28a**). The result of this conditioning dramatically increased the 2D effective affinity of the WP P14 cells to the level of RP P14 cells. Furthermore, $CD4^{+}FoxP3^{+}$ regulatory T cells (Tregs) play an important in downplaying the effector function of $CD8^{+}$ T cells and with this rationale, ablation of Tregs were undertaken (**Figure 28b**). Specifically removing Tregs resulted in the dramatic increase of the 2D effective affinity of P14 cells from WP similar to the values observed of T cells from RP.

Tregs plan an important role in regulation of immune response mediated either through direct contact or via protein secretion and that can potentially have an impact regulating the 2D effective affinity of CD8+ T cells found in the WP. To address whether transforming growth factor (TGF-β) secretion, an influential cytokine known to play pleiotropic role in the control of T cell immune response [73] and modulation of Treg function [74], blocking of TGF-β using specific inhibitor (SB431542) in mice and subsequently measuring kinetics of P14 cells from respective compartments was conducted (**Figure 28c**). This resulted in observation of no differences seen between the P14 cells from WP and the RP, as the P14 cells from WP had an elevated 2D effective affinity similar to that of the P14 cells found in RP. Additionally, *in vitro* treatment of RP P14 cells following 11 dpi exhibited lower 2D effective affinity when compared to no treatment. Similarly treated 7 dpi RP P14 cells did not lower the 2D effective affinity when compared to that of 7 dpi RP P14 cells with no *in vitro* conditioning.

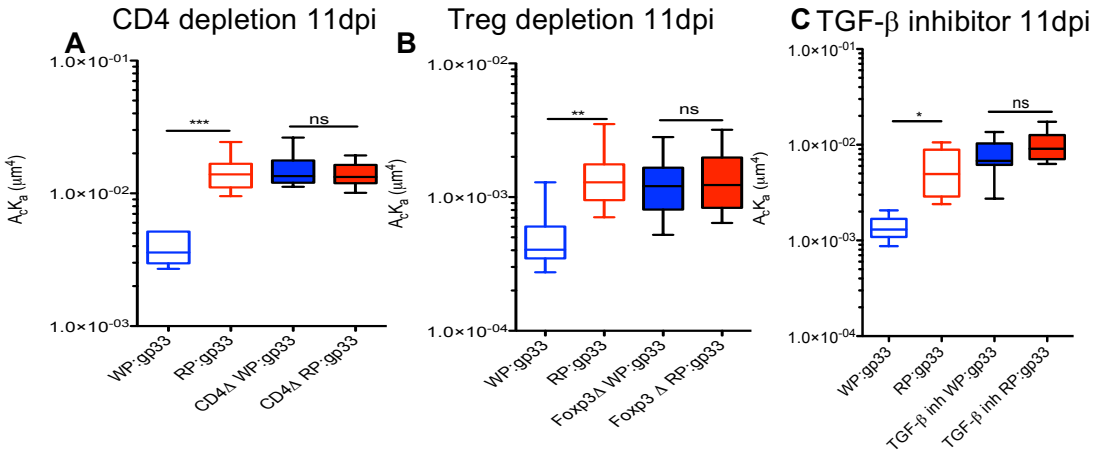

Figure 28. Localized components regulates P14 T cells. (A) Ablation of $CD4^+$ T cells by GK 1.5 antibody to mice infected with LCMV abolished the differences between the P14 cells from different compartments 11dpi. (B) Similarly, adoptively transferred P14 T cells into FoxP3-DTR mice also exhibited no differences between the two compartments by removal of $FoxP3^+$ cells from the host. (C) TGF-β inhibitory drug treatment to mice infected with LCMV also abolished differences seen when compared to that of the untreated mice.

5.2.5 *in vitro* conditioning of anatomic compartmentalization $CD8^+$ T cells regulating 2D effective affinity during early immune contraction phase

Understanding the effects stemming from Tregs and TGF-β, rather than separately done so from the *in vivo* experiments, *in vitro* experiment involving incubation with Tregs and blocking antibodies targeting TGF-β were conducted. Incubation of RP P14 cells following 10dpi along with Tregs in the presence and absence of TGF-β for 24 hrs provided a more in-depth interconnection of the two composition on the effect on 2D effective affinity (**Figure 29**). As observed by the *in vivo* experiment involving ablation of the Treg, incubation of Treg with RP decreased the 2D effective affinity, while blocking TGF-β alongside with Treg did not impact the 2D effective affinity compared to that of the no treatment. These results suggest that Tregs and TGF-β are primarily involved in influencing

the 2D effective affinity for antigen-specific T cells found in WP during the early contraction phase of the immune response.

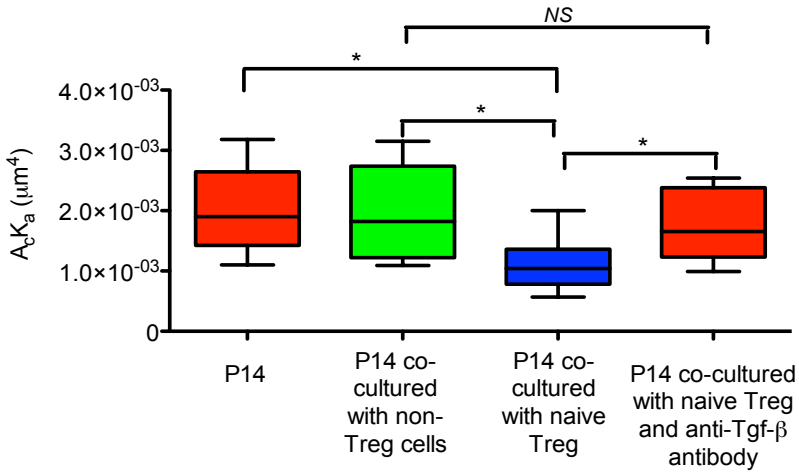

Figure 29. *in vitro* conditioning of RP P14. Following 10dpi, P14 cells were conditioned with various components to understand the role of each components influencing 2D effective binding affinity.

5.2.6 Post-translational modification and membrane organizing effect on anatomically compartmentalized CD8$^+$ T cells

Cytokine influence has been shown to cause post-translational modification, especially regulating plasma membrane clustering [75]. As such, P14 T cells were subjected to *in vitro* treatment focused on cluster membrane organization. Cells sorted from RP and WP were treated with nystatin to sequester lipid raft or treated with cholesterol oxidase to remove cholesterol (**Figure 30 a and b**). Thereby, such treatments following TCR interaction will prevent formation of cluster to take place and observe the effect on their respective 2D effective affinities. Following such post-translational modification, we observed that no differences were observed between P14 cells from RP and WP. Interestingly, the treatment of RP cells decreased the 2D effective affinity when compared to that of the no treatment done to RP P14 cells. To rule out other post-translational modifications, P14 T cells were subjected to deglycosylation by PNgase F treatment was also condcuted (**Figure 30c**). This resulted in the same difference observed when compared

to that of the untreated. Altogether, release of TGF-β by Tregs could poetntially inhibit lipid raft formation, thereby inhibiting increased 2D effective affinity, a mechanism potentially inherent to prevent excessive damage to the surrounding tissue.

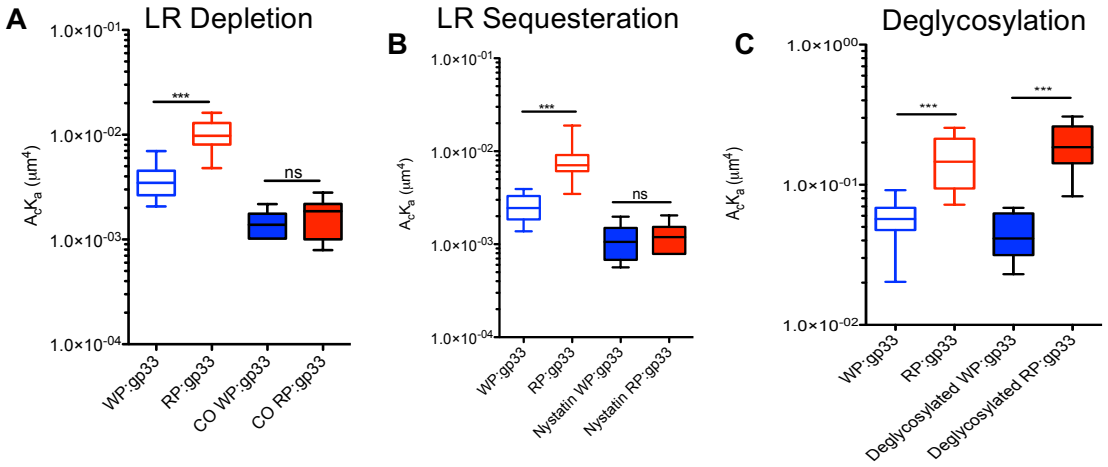

Figure 30. Post-translation modification treatment on P14 T cells. (A and B) P14 T cells were treated with membrane disrupting drug to inhibit the effect lipid raft cluster formation of sorted samples following 11dpi. Following treatment, both conditions exhibit a decreased 2D effective binding affinity. (C) Sorted P14 cells following 11dpi were deglycosylated and did not affect the 2D effective binding affinity.

5.2.7 Cluster-induced 2D binding affinity of memory marker specific T cells

Further investigation into the type of T cells that are exhibiting increased 2D effective affinities, P14 following 11 dpi were sorted based on memory markers to understand the role of various subsets of antigen experienced cells respective to their anatomical location. Early effector (KLRG1^{high}/CD127^{low}; SLEC) and memory (KLRG1^{low}/CD127^{high}; MPEC) precursor marker cells from both WP and RP were sorted to understand how the anatomical location of these subsets of cells influence their binding kinetics (**Figure 31**). Cells sorted based on memory markers from RP had two differing 2D effective affinities populations, specifically, SLECs display increased 2D effective affinity when compared to that of the MPECs from the same compartment. However, the effector markers pertaining to WP location exhibited different binding kinetics to the same

subset of cells found in RP. The population pertaining to the SLEC markers did not exhibit a higher 2D effective affinity when compared to that of the MPECs found in WP.

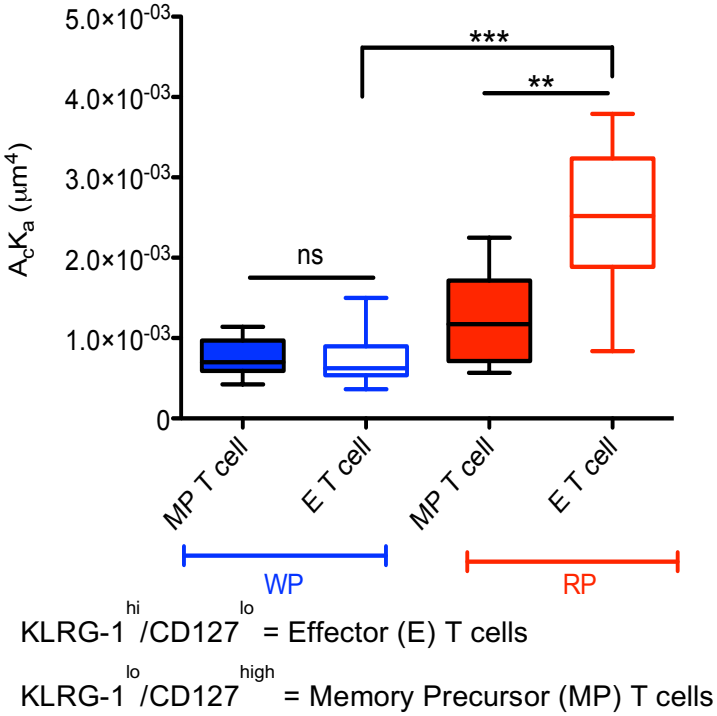

Figure 31. Memory marker specific T cells role in 2D kinetics. P14 cells sorted based on anatomically localized compartments and on memory markers expression following 11dpi.

5.3 Discussion

Host immune response to viral infection induces a T cell activation of cognate specific T cells for expansion to efficiently recognize to clear viral infection. An increased frequency of high affinity subset of clones provides effective clearance of the virus, particularly in the case when viral mutations occurring to escape from the $CD8^+$ T cell response. Indeed, occurrence of viral escape mutants take place during the contraction phase of the immune response, following the peak of viremia [76]. The precise timing of generation of viral mutations indicate the cost of viral fitness, and coincidentally, an increased 2D effective binding affinity from RP and the vasculature network occurs during the early contraction phase. Therefore, during early contraction

phase, the increase in 2D recognition provides insight on development of novel strategies to combat persistent viral infections.

Conventionally, when analyzing cells in organs, many studies rely on the entirety of the organ rather than segregating the compartments based on the anatomy of the organ (tissue embedded vs. circulating). Therefore, it is important to dissect where, when, and how viral specific T cells respond within the spleen. By allowing to analyze cells from compartments provides insight on how the microenvironment influences major leukocyte markers, kinetics and activity that might otherwise conflate interpretation of between localization vs. the organ itself. Regardless of the memory markers, what was observed using 2D assay is that phenotypic markers alone do not exhibit certain activity, as the anatomical localization of the cells within the organ, in addition to phenotypic markers, regulate cellular kinetics. Furthermore, cellular and protein compositions that constitutes the localized site regulates TCR-pMHC interaction, suggesting these compositions found particularly in WP plays a central role in establishing long-term memory subsets. Whereas in the absence of these compositions, expanded $CD8^+$ T cells are short lived in the periphery. Regulation of cellular and protein components, such as TGF-β and Treg, has influences CD8+ T cell response in many diseases and influences [77-80]. Additionally, cytokines have shown to influence post-translation modification of protein to regulate cellular trafficking [81]. Post-translation modification, including cholesterol membrane clustering of TCR, has been influential in signaling for T cells [82-87]. As such, local compositions that are compartmentalized can regulate membrane cholesterol level in regulating TCR-pMHC interaction that can implicate the outcome of various diseases. T-cells from spleen was sorted based on compartments and then by marker expression within their respective compartment. Marker expression on cells were used sorted to the following subsets: SLECs and MPECs, which is capable of generating long-lived memory $CD8^+$ T cells (central and effector memory T cells) [8].

As MPECs found in WP are continuously interacting with antigen, this provides an environment to potentially downregulating their effector functions due to immune regulating compositions in WP and when SLECs or effector cells from RP enter into WP, the continuous interaction with antigen could eventually lead to functional exhaustion due to heightened 2D effective binding affinity [88]. Because of high rate of interaction with antigen in WP than in RP, both MPEC and SLEC found in WP behave the same.

Over the course of acute infection, MPECs found in RP are driven towards differentiating to SLECs or effector cells due to repetitive antigenic interactions in peripheral sites (but not continuously as would be in the case in WP) [88] and some MPECs just entering into RP from the WP, which could be the reason for the heterogeneous population in RP being observed. It is also shown through 2D measurement that SLECs in RP have higher affinity than MPECs found in RP. These results highlight that intricate regulation of T cell function and fate is determined by anatomic compartmentalization during the early immune contraction phase.

In summary, this study has shown that anatomical compartmentalization of $CD8^+$ T cells plays an important role in establishing the lineage and activity of the cell, especially their recognition. Interestingly, during early contraction phase of the immune response, peripheral $CD8^+$ T cell experiences an increased sensitivity to recognize minute antigen levels and mutant viral epitopes to prevent persistent infection to take place. These results provide insights and implications in developing novel approaches to intervene infectious, cancer, and autoimmune disorders over the course of these diseases.

CHAPTER 6

CONCLUSIONS AND FUTURE DIRECTIONS

The thesis on analyzing kinetic parameters on CTL in the context of viral infection encompasses utilizing biophysical assays to understand the interaction between TCR and pMHC. Firstly, we demonstrated how private dominant polyclonal antigen-specific T cell interacts with both the WT and variants by using CMV model and we have shown that sensitivity with 2D biophysical assays provides binding kinetics and insight far better than 3D conventional assays [49]. Provided these cells are experiencing force from its environment, we have shown how the interaction (bond lifetime) between the TCR and pMHC (both WT and variants) are influenced under various force clamps. Unlike integrins, which exists in multiple states, associates with various lifetime events that can be addressed as a two-state model [89]. However, no known multiple states of TCR has been shown, yet we observed two state fit for the survival frequency for polyclonal enriched NLV-specific T cells binding to NLV peptide using mutant MHC, which abolishes CD8 binding to MHC (**Figure 32**). Interestingly, this two state fitting exhibited only at the non-critical force, and at the critical force a single state fit was achieved. This could potentially imply that mobility might exist of the peptide in the MHC groove that could translate its mobility to TCR (or certain domains of CDR loops)

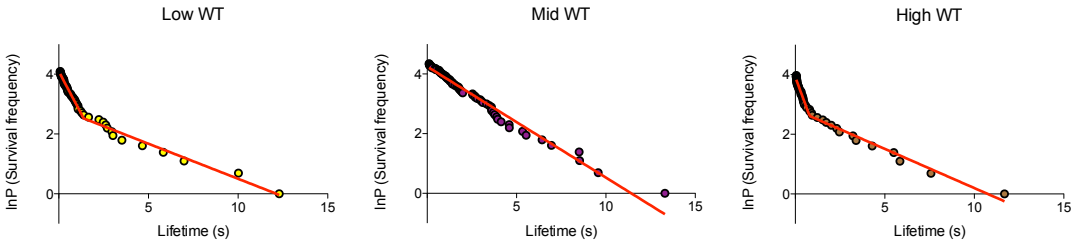

Figure 32. Analysis of lifetime bonds of TCR-pMHC of CMV polyclonal cells. Plots of survival frequency versus lifetime data and the two-state fitting (solid red line). Lifetime distribution from critical force, force clamped higher than critical force, and force clamped lower than critical force.

when the peptide interfaces with TCR [90]. This mobility that exists between the two proteins could potentially be stabilized at the critical force, which could imply the most optimal state to induce signaling to the T cell.

Characterizing kinetic parameters of the CMV has established a ground work on understanding polyclonal T cell interaction with both WT and mutant variants. However, we utilized certain mutants to understand the importance of various interaction between TCR and pMHC. In the case of HCV, hydrogen bonds between pMHC and TCR has been highlighted [91] and the importance of characterizing viral persistence in the case of HCV and HIV will provide novel and applicable insights on how to intervene using new methodologies to boost recognition and signaling for effective viral clearance. Specifically, in the case of HCV, multiple single mutant variants has been shown that rises from the error-prone RNA polymerase, as well as double mutants [92-96]. Characterizing these mutations will provide unique methodologies to create optimal chimeric antigen receptor to intervene and induce an efficient signal to generate a functional lysis response, thereby eliminating escape mutants stemming from these persistent viral infections, like HCV [97].

In regards to future directions of LCMV study, we could extend into understanding the gene profile that influences enhanced 2D effective affinity seen for the antigen specific T cells from the RP. Based on our indication, these genes should have influence in membrane cluster formation, in addition to the subset it is categorized as MPEC or SLEC. Squalene injection of $CD4^+$ T cell has shown to induce increased membrane cholesterol and diverting towards an inflammatory response and this direction has influenced increase T-bet expression [98]. Increased T-bet expression is seen for cells in the SLEC lineage and this increased T-bet is linked to an IL-12 cytokine response and increased IFN-γ and granzyme B [8, 99], thereby, worth investigating the effects of IL-12 effect on TCR-pMHC 2D effective binding affinity. Our preliminary data indicates by T-bet transduction using T-bet DNA fragment sub-cloned into pGC-FU lentiviral vector

containing GFP to generate a recombinant lentiviral vector that over-express T-bet transcription factor. Additionally, a control pGC-Fu lentiviral vector containing GFP with no T-bet DNA fragment was also generated. Following 7dpi, when T cells from both compartments exhibited comparable 2D effective affinity, adoptively transferred collective P14 T cells from the spleen were sorted and transduced with the lentivirus overnight. Followed by 2D micropipette adhesion frequency assay resulted in T-cells over-expressing T-bet exhibited 2-times increased binding affinity than control transfection (**Figure 33a)**. Following transduction to over-express T-bet resulted in lower TCR expression (**Figure 33b**). Future direction could involve to segregate the two compartments from 11dpi samples and potentially might expect in the case if 11dpi RP has already increased T-bet, treating the RP T cells with the lentivirus to over-express T-bet might not indicate a big difference when compared to untreated RP T cells.

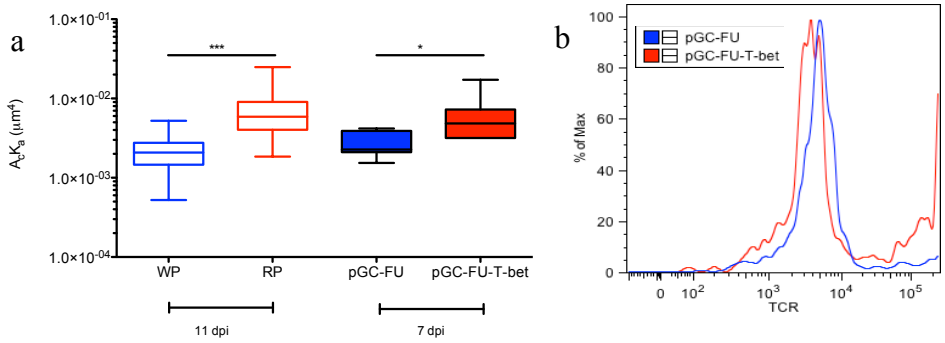

Figure 33. T-bet transduction on T cells. (a) Comparison of 11dpi samples sorted from their respective compartments and to of spleoncytes from 7dpi with T-bet or control transduction. (b) TCR expression between cells transduced with T-bet or control.

Along the line of LCMV study, we focused on acute infection role on anatomic compartmentalization of T cells. Following LCMV Armstrong infection, this viral strain exhibit distinct tropisms within the RP, which explains an increase of antigen specific T cells found in the RP [100, 101]. Whereas LCVM Clone 13 strain, which induces chronic infection, prefers the WP for its tropical location and could explain the induction leading to disruption of generating a proper immune response, in which case the infection

could result in exhausting the adaptive immune response and fail to facilitate viral clearance [100, 102].

Overall, this study has initiated using biophysical methodologies to study how immune responds upon viral infection and how virus takes advantage of the natural phenomenon of the host to use it to it owns advantage for its persistence and possibly leading detrimental result of the host, in the case of viral mutations. However, this project can be expanded beyond the scope by looking into other infections as the assays used in this project provide unique data readouts and experimental setup. One intriguing field is in autoimmune disease, human immunodeficiency virus as an example or even autoimmune hepatitis, to understand kinetics of immune response leading to the loss of differentiating between viral proteins and endogenous proteins of the host. Furthermore, understanding the kinetics involved in initiating an effective immune response mediated by $CD8^+$ T cells and how that shapes up the immune system provides insight on interventions.

REFERENCES

1. Blakely, B.L., et al., *A DNA-based molecular probe for optically reporting cellular traction forces.* Nat Methods, 2014. **11**(12): p. 1229-32.

2. Zhang, Y., et al., *DNA-based digital tension probes reveal integrin forces during early cell adhesion.* Nat Commun, 2014. **5**: p. 5167.

3. Anderson, K.G., et al., *Intravascular staining for discrimination of vascular and tissue leukocytes.* Nature Protocols, 2014. **9**(1): p. 209-222.

4. Hubbell, J.A., S.N. Thomas, and M.A. Swartz, *Materials engineering for immunomodulation.* Nature, 2009. **462**(7272): p. 449-460.

5. Thomas, W.E., *Mechanochemistry of receptor-ligand bonds.* Current opinion in structural biology, 2009. **19**(1): p. 50-55.

6. Bowen, D.G. and C.M. Walker, *Adaptive immune responses in acute and chronic hepatitis C virus infection.* Nature, 2005. **436**(7053): p. 946-52.

7. Davies, L.C., et al., *Tissue-resident macrophages.* Nat Immunol, 2013. **14**(10): p. 986-95.

8. Lazarevic, V., L.H. Glimcher, and G.M. Lord, *T-bet: a bridge between innate and adaptive immunity.* Nat Rev Immunol, 2013. **13**(11): p. 777-89.

9. Homann, D., L. Teyton, and M.B. Oldstone, *Differential regulation of antiviral T-cell immunity results in stable CD8+ but declining CD4+ T-cell memory.* Nat Med, 2001. **7**(8): p. 913-9.

10. van de Sandt, C.E., J.H. Kreijtz, and G.F. Rimmelzwaan, *Evasion of influenza A viruses from innate and adaptive immune responses.* Viruses, 2012. **4**(9): p. 1438-76.

11. Hadrup, S.R. and T.N. Schumacher, *MHC-based detection of antigen-specific CD8+ T cell responses.* Cancer Immunology, Immunotherapy, 2010. **59**(9): p. 1425-1433.

12. Chaplin, D.D., *Overview of the immune response.* J Allergy Clin Immunol, 2010. **125**(2 Suppl 2): p. S3-23.

13. Duan, S. and P.G. Thomas, *Balancing Immune Protection and Immune Pathology by CD8(+) T-Cell Responses to Influenza Infection.* Front Immunol, 2016. **7**: p. 25.

14. Arens, R. and S.P. Schoenberger, *Plasticity in programming of effector and memory CD8 T-cell formation.* Immunol Rev, 2010. **235**(1): p. 190-205.

15. Kalejta, R.F., *Tegument proteins of human cytomegalovirus.* Microbiology and Molecular Biology Reviews, 2008. **72**(2): p. 249-265.

16. Thimme, R., M. Binder, and R. Bartenschlager, *Failure of innate and adaptive immune responses in controlling hepatitis C virus infection.* FEMS microbiology reviews, 2012. **36**(3): p. 663-683.

17. Roy, C.R., *Immunology: professional secrets.* Nature, 2003. **425**(6956): p. 351-352.

18. Trapani, J.A. and M.J. Smyth, *Functional significance of the perforin/granzyme cell death pathway.* Nat Rev Immunol, 2002. **2**(10): p. 735-47.

19. Tattevin, P., et al., *Increasing incidence of severe Epstein-Barr virus-related infectious mononucleosis: surveillance study.* J Clin Microbiol, 2006. **44**(5): p. 1873-4.

20. Manicklal, S., et al., *The "silent" global burden of congenital cytomegalovirus.* Clin Microbiol Rev, 2013. **26**(1): p. 86-102.

21. Verstrepen, B.E., A. Boonstra, and G. Koopman, *Immune mechanisms of vaccine induced protection against chronic hepatitis C virus infection in chimpanzees.* World J Hepatol, 2015. **7**(1): p. 53-69.

22. Terilli, R.R. and A.L. Cox, *Immunity and hepatitis C: a review.* Curr HIV/AIDS Rep, 2013. **10**(1): p. 51-8.

23. Gayle, H.D. and G.L. Hill, *Global impact of human immunodeficiency virus and AIDS.* Clin Microbiol Rev, 2001. **14**(2): p. 327-35.

24. Alcami, A., P. Ghazal, and J.W. Yewdell, *Viruses in control of the immune system. Workshop on molecular mechanisms of immune modulation: lessons from viruses.* EMBO Rep, 2002. **3**(10): p. 927-32.

25. Wherry, E.J., et al., *Viral persistence alters CD8 T-cell immunodominance and tissue distribution and results in distinct stages of functional impairment.* J Virol, 2003. **77**(8): p. 4911-27.

26. Yi, J.S., M.A. Cox, and A.J. Zajac, *T-cell exhaustion: characteristics, causes and conversion.* Immunology, 2010. **129**(4): p. 474-81.

27. Bowen, D.G. and C.M. Walker, *Adaptive immune responses in acute and chronic hepatitis C virus infection.* Nature, 2005. **436**(7053): p. 946-952.

28. Plauzolles, A., M. Lucas, and S. Gaudieri, *Hepatitis C virus adaptation to T-cell immune pressure.* ScientificWorldJournal, 2013. **2013**: p. 673240.

29. Burke, K.P. and A.L. Cox, *Hepatitis C virus evasion of adaptive immune responses: a model for viral persistence.* Immunol Res, 2010. **47**(1-3): p. 216-27.

30. Ashfaq, U.A., et al., *An overview of HCV molecular biology, replication and immune responses.* Virol J, 2011. **8**: p. 161.

31. Berkhoff, E.G., et al., *The loss of immunodominant epitopes affects interferon-gamma production and lytic activity of the human influenza virus-specific cytotoxic T lymphocyte response in vitro.* Clin Exp Immunol, 2007. **148**(2): p. 296-306.

32. Iwasaki, A., *Antiviral immune responses in the genital tract: clues for vaccines.* Nat Rev Immunol, 2010. **10**(10): p. 699-711.

33. Zhou, X., et al., *Role of lymphocytic choriomeningitis virus (LCMV) in understanding viral immunology: past, present and future.* Viruses, 2012. **4**(11): p. 2650-69.

34. Wherry, E.J. and R. Ahmed, *Memory CD8 T-cell differentiation during viral infection.* J Virol, 2004. **78**(11): p. 5535-45.

35. Gui, J., et al., *MCL1 enhances the survival of CD8+ memory T Cells after viral infection.* J Virol, 2015. **89**(4): p. 2405-14.

36. Kaech, S.M., et al., *Selective expression of the interleukin 7 receptor identifies effector CD8 T cells that give rise to long-lived memory cells.* Nat Immunol, 2003. **4**(12): p. 1191-8.

37. Griffiths, P.D. and J.E. Grundy, *Molecular biology and immunology of cytomegalovirus.* Biochem. J, 1987. **241**: p. 313-324.

38. Davidson, B.L. and X.O. Breakefield, *Viral vectors for gene delivery to the nervous system.* Nat Rev Neurosci, 2003. **4**(5): p. 353-64.

39. Kunz, S., et al., *Molecular analysis of the interaction of LCMV with its cellular receptor Œ±-dystroglycan.* The Journal of cell biology, 2001. **155**(2): p. 301-310.

40. Butz, E.A. and M.J. Bevan, *Massive expansion of antigen-specific CD8+ T cells during an acute virus infection.* Immunity, 1998. **8**(2): p. 167-75.

41. Wikoff, W.R., et al., *Response and recovery in the plasma metabolome tracks the acute LCMV-induced immune response.* J Proteome Res, 2009. **8**(7): p. 3578-87.

42. Ruddle, N.H. and E.M. Akirav, *Secondary lymphoid organs: responding to genetic and environmental cues in ontogeny and the immune response.* J Immunol, 2009. **183**(4): p. 2205-12.

43. Junt, T., E. Scandella, and B. Ludewig, *Form follows function: lymphoid tissue microarchitecture in antimicrobial immune defence.* Nat Rev Immunol, 2008. **8**(10): p. 764-75.

44. Yi, T. and J.G. Cyster, *EBI2-mediated bridging channel positioning supports splenic dendritic cell homeostasis and particulate antigen capture.* Elife, 2013. **2**: p. e00757.

45. Bronte, V. and M.J. Pittet, *The spleen in local and systemic regulation of immunity.* Immunity, 2013. **39**(5): p. 806-18.

46. Gairin, J.E., et al., *Optimal lymphocytic choriomeningitis virus sequences restricted by H-2Db major histocompatibility complex class I molecules and presented to cytotoxic T lymphocytes.* J Virol, 1995. **69**(4): p. 2297-305.

47. Shorter, S.K., et al., *Viral Escape Mutant Epitope Maintains TCR Affinity for Antigen yet Curtails CD8 T Cell Responses.* PLoS One, 2016. **11**(2): p. e0149582.

48. Purbhoo, M.A., et al., *The human CD8 coreceptor effects cytotoxic T cell activation and antigen sensitivity primarily by mediating complete phosphorylation of the T cell receptor zeta chain.* J Biol Chem, 2001. **276**(35): p. 32786-92.

49. Gras, S., et al., *Structural bases for the affinity-driven selection of a public TCR against a dominant human cytomegalovirus epitope.* J Immunol, 2009. **183**(1): p. 430-7.

50. Zaia, J.A., et al., *Infrequent occurrence of natural mutations in the pp65(495-503) epitope sequence presented by the HLA A*0201 allele among human cytomegalovirus isolates.* J Virol, 2001. **75**(5): p. 2472-4.

51. Dialynas, D.P., et al., *Characterization of the murine T cell surface molecule, designated L3T4, identified by monoclonal antibody GK1.5: similarity of L3T4 to the human Leu-3/T4 molecule.* J Immunol, 1983. **131**(5): p. 2445-51.

52. Dialynas, D.P., et al., *Characterization of the murine antigenic determinant, designated L3T4a, recognized by monoclonal antibody GK1.5: expression of L3T4a by functional T cell clones appears to correlate primarily with class II MHC antigen-reactivity.* Immunol Rev, 1983. **74**: p. 29-56.

53. Wilde, D.B., et al., *Evidence implicating L3T4 in class II MHC antigen reactivity; monoclonal antibody GK1.5 (anti-L3T4a) blocks class II MHC antigen-specific proliferation, release of lymphokines, and binding by cloned murine helper T lymphocyte lines.* J Immunol, 1983. **131**(5): p. 2178-83.

54. Matloubian, M., R.J. Concepcion, and R. Ahmed, *CD4+ T cells are required to sustain CD8+ cytotoxic T-cell responses during chronic viral infection.* J Virol, 1994. **68**(12): p. 8056-63.

55. Huang, J., et al., *The kinetics of two-dimensional TCR and pMHC interactions determine T-cell responsiveness.* Nature, 2010. **464**(7290): p. 932-936.

56. Huang, J., et al., *Kinetics of MHC-CD8 interaction at the T cell membrane.* The Journal of Immunology, 2007. **179**(11): p. 7653-7662.

57. Jiang, N., et al., *Two-stage cooperative T cell receptor-peptide major histocompatibility complex-CD8 trimolecular interactions amplify antigen discrimination.* Immunity, 2011. **34**(1): p. 13-23.

58. Evans, E., K. Ritchie, and R. Merkel, *Sensitive force technique to probe molecular adhesion and structural linkages at biological interfaces.* Biophys J, 1995. **68**(6): p. 2580-7.

59. Heinrich, V., A. Leung, and E. Evans, *Nano-to-microscale mechanical switches and fuses mediate adhesive contacts between leukocytes and the endothelium.* J Chem Inf Model, 2005. **45**(6): p. 1482-90.

60. Chung, K., et al., *Imaging single-cell signaling dynamics with a deterministic high-density single-cell trap array.* Anal Chem, 2011. **83**(18): p. 7044-52.

61. Chingozha, L., et al., *A generalizable, tunable microfluidic platform for delivering fast temporally varying chemical signals to probe single-cell response dynamics.* Anal Chem, 2014. **86**(20): p. 10138-47.

62. Edelstein, A., *Re-thinking typologies of multiple murders: the missing category of serial-mass murder and its theoretical and practical implications.* Int J Emerg Ment Health, 2014. **16**(2): p. 350-3.

63. Tomek, J., O. Novak, and J. Syka, *Two-Photon Processor and SeNeCA: a freely available software package to process data from two-photon calcium imaging at speeds down to several milliseconds per frame.* J Neurophysiol, 2013. **110**(1): p. 243-56.

64. Kirimli, C.E., W.H. Shih, and W.Y. Shih, *DNA hybridization detection with 100 zM sensitivity using piezoelectric plate sensors with an improved noise-reduction algorithm.* Analyst, 2014. **139**(11): p. 2754-63.

65. Hong, J., et al., *Force-Regulated In Situ TCR-Peptide-Bound MHC Class II Kinetics Determine Functions of CD4+ T Cells.* J Immunol, 2015. **195**(8): p. 3557-64.

66. Liu, B., et al., *Accumulation of dynamic catch bonds between TCR and agonist peptide-MHC triggers T cell signaling.* Cell, 2014. **157**(2): p. 357-68.

67. Lachmann, R., et al., *Polyfunctional T cells accumulate in large human cytomegalovirus-specific T cell responses.* J Virol, 2012. **86**(2): p. 1001-9.

68. Trautmann, L., et al., *Selection of T cell clones expressing high-affinity public TCRs within Human cytomegalovirus-specific CD8 T cell responses.* J Immunol, 2005. **175**(9): p. 6123-32.

69. Liu, B., et al., *2D TCR-pMHC-CD8 kinetics determines T-cell responses in a self-antigen-specific TCR system.* Eur J Immunol, 2014. **44**(1): p. 239-50.

70. Sabatino, J.J., Jr., et al., *High prevalence of low affinity peptide-MHC II tetramer-negative effectors during polyclonal CD4+ T cell responses.* J Exp Med, 2011. **208**(1): p. 81-90.

71. Shin, H., et al., *Viral antigen and extensive division maintain virus-specific CD8 T cells during chronic infection.* J Exp Med, 2007. **204**(4): p. 941-9.

72. Mueller, S.N. and R.N. Germain, *Stromal cell contributions to the homeostasis and functionality of the immune system.* Nat Rev Immunol, 2009. **9**(9): p. 618-29.

73. Li, M.O. and R.A. Flavell, *TGF-beta: a master of all T cell trades.* Cell, 2008. **134**(3): p. 392-404.

74. Chen, W., et al., *Conversion of peripheral CD4+CD25- naive T cells to CD4+CD25+ regulatory T cells by TGF-beta induction of transcription factor Foxp3.* J Exp Med, 2003. **198**(12): p. 1875-86.

75. Yamazaki, S., et al., *TGF-beta as a candidate bone marrow niche signal to induce hematopoietic stem cell hibernation.* Blood, 2009. **113**(6): p. 1250-6.

76. Goulder, P.J. and D.I. Watkins, *HIV and SIV CTL escape: implications for vaccine design.* Nat Rev Immunol, 2004. **4**(8): p. 630-40.

77. Hervas-Stubbs, S., et al., *Direct effects of type I interferons on cells of the immune system.* Clin Cancer Res, 2011. **17**(9): p. 2619-27.

78. Richer, M.J., J.C. Nolz, and J.T. Harty, *Pathogen-specific inflammatory milieux tune the antigen sensitivity of CD8(+) T cells by enhancing T cell receptor signaling.* Immunity, 2013. **38**(1): p. 140-52.

79. Marshall, H.D., et al., *IFN-alpha beta and self-MHC divert CD8 T cells into a distinct differentiation pathway characterized by rapid acquisition of effector functions.* J Immunol, 2010. **185**(3): p. 1419-28.

80. Marshall, H.D., S.L. Urban, and R.M. Welsh, *Virus-induced transient immune suppression and the inhibition of T cell proliferation by type I interferon.* J Virol, 2011. **85**(12): p. 5929-39.

81. Nolz, J.C. and J.T. Harty, *IL-15 regulates memory CD8+ T cell O-glycan synthesis and affects trafficking.* J Clin Invest, 2014. **124**(3): p. 1013-26.

82. Xavier, R., et al., *Membrane compartmentation is required for efficient T cell activation.* Immunity, 1998. **8**(6): p. 723-32.

83. Janes, P.W., et al., *The role of lipid rafts in T cell antigen receptor (TCR) signalling.* Semin Immunol, 2000. **12**(1): p. 23-34.

84. Kabouridis, P.S., et al., *Cholesterol depletion disrupts lipid rafts and modulates the activity of multiple signaling pathways in T lymphocytes.* Eur J Immunol, 2000. **30**(3): p. 954-63.

85. Fahmy, T.M., et al., *Increased TCR avidity after T cell activation: a mechanism for sensing low-density antigen.* Immunity, 2001. **14**(2): p. 135-43.

86. Slifka, M.K. and J.L. Whitton, *Functional avidity maturation of CD8(+) T cells without selection of higher affinity TCR.* Nat Immunol, 2001. **2**(8): p. 711-7.

87. Tuosto, L., et al., *Organization of plasma membrane functional rafts upon T cell activation.* Eur J Immunol, 2001. **31**(2): p. 345-9.

88. Yuzefpolskiy, Y., et al., *Early CD8 T-cell memory precursors and terminal effectors exhibit equipotent in vivo degranulation.* Cell Mol Immunol, 2015. **12**(4): p. 400-8.

89. Chen, W., et al., *Observing force-regulated conformational changes and ligand dissociation from a single integrin on cells.* J Cell Biol, 2012. **199**(3): p. 497-512.

90. Hawse, W.F., et al., *TCR scanning of peptide/MHC through complementary matching of receptor and ligand molecular flexibility.* J Immunol, 2014. **192**(6): p. 2885-91.

91. Nivarthi, U.K., et al., *An extensive antigenic footprint underpins immunodominant TCR adaptability against a hypervariable viral determinant.* J Immunol, 2014. **193**(11): p. 5402-13.

92. Urbani, S., et al., *The impairment of CD8 responses limits the selection of escape mutations in acute hepatitis C virus infection.* J Immunol, 2005. **175**(11): p. 7519-29.

93. Cox, A.L., et al., *Cellular immune selection with hepatitis C virus persistence in humans.* J Exp Med, 2005. **201**(11): p. 1741-52.

94. Chang, K.M., et al., *Immunological significance of cytotoxic T lymphocyte epitope variants in patients chronically infected by the hepatitis C virus.* J Clin Invest, 1997. **100**(9): p. 2376-85.

95. Spangenberg, H.C., et al., *Intrahepatic CD8+ T-cell failure during chronic hepatitis C virus infection.* Hepatology, 2005. **42**(4): p. 828-37.

96. Penna, A., et al., *Dysfunction and functional restoration of HCV-specific CD8 responses in chronic hepatitis C virus infection.* Hepatology, 2007. **45**(3): p. 588-601.

97. Sautto, G.A., et al., *Chimeric antigen receptor (CAR)-engineered T cells redirected against hepatitis C virus (HCV) E2 glycoprotein.* Gut, 2016. **65**(3): p. 512-23.

98. Surls, J., et al., *Increased membrane cholesterol in lymphocytes diverts T-cells toward an inflammatory response.* PLoS One, 2012. **7**(6): p. e38733.

99. Joshi, N.S., et al., *Inflammation directs memory precursor and short-lived effector CD8(+) T cell fates via the graded expression of T-bet transcription factor.* Immunity, 2007. **27**(2): p. 281-95.

100. Smelt, S.C., et al., *Differences in affinity of binding of lymphocytic choriomeningitis virus strains to the cellular receptor alpha-dystroglycan correlate with viral tropism and disease kinetics.* J Virol, 2001. **75**(1): p. 448-57.

101. Dauner, J.G., I.R. Williams, and J. Jacob, *Differential microenvironment localization of effector and memory CD8 T cells.* J Immunol, 2008. **180**(1): p. 291-9.

102. Mueller, S.N., et al., *Viral targeting of fibroblastic reticular cells contributes to immunosuppression and persistence during chronic infection.* Proc Natl Acad Sci U S A, 2007. **104**(39): p. 15430-5.